ATTEMPTS TOWARD MACHINING OF THE BACK SURFACE OF SI SUBSTRATE USING INFRARED FEMTOSECOND LASER

Student name: LUONG PHU KHANH
Supervisor: Prof. YAMADA NOBORU
Prof. ITO YOSHIRO

Doctor Dissertation
Energy and Environment Science
Nagaoka University of Technology

April 16, 2020

Table of Contents

Acknowledgements

This thesis is the summary of the research results of 5 years in the Ph.D. course at the Nagaoka University of Technology with the precious supervision of Professor Ito Yoshiro and Professor Yamada Noboru. I would like to express my gratitude to these two great professors, who gave me guidance, suggestions for my research and support my living in Japan. Thank you for giving me a chance to study under your supervision.

I want to thank Associate Professor Yamagishi Rie for your helpful comment and many useful suggestions for my research. Thanks to other lab's member for your help and for sharing the beautiful life in Japan.

I express great appreciation to the Nagaoka University of Technology, where I received an education.

Finally, I would love to give many thanks to my family.

LUONG PHU KHANH

April 2020

Publications

Scientific Journals

[1] **K. P. Luong**, R. Tanabe- Yamagishi, N. Yamada, and Y. Ito, "Micromachining of The Back Surface and Interior of Si Using Infrared Femtosecond Laser Pulses", *Journal of Laser Applications,* Vol. 32 (012017), published February 19th, 2020. https://doi.org/10.2351/1.5123309

[2] **K. P. Luong**, R. Tanabe- Yamagishi, N. Yamada, and Y. Ito, "Laser-Assisted Wet Etching of Silicon Back Surfaces Using 1552 nm Femtosecond Laser", *International Journal of Electrical Machining*, No. 25, pp. 7-13, published March, 2020.

Abstract

This paper reports the attempts to machine the back surface of Si using a femtosecond laser at a wavelength of 1,552.5-nm. As Si is optically transparent at this wavelength, I attempted to machine the back surface and interior of a Si substrate by a non-linear absorption process, similar to the non-linear process used to treat dielectric materials using visible and near-infrared ultra-short lasers. The femtosecond laser impinged on the front surface of the Si substrate and was focused at or near the back surface. I scanned the laser beam linearly along the back surface at different scan speeds and repetition rates at several focus positions. Changes occurring on the back surface were observable by visible optical microscopy and scanning electron microscopy, whereas those in the interior of Si were observable only by infrared microscopy. Meanwhile, no change was detected on the front surface where the laser impinged. After a certain period, the point of irradiation showed changes; afterwards, changes in the interior of Si began to occur continuously. However, the changes on the back surface occurred in a rather discrete manner, observed intermittently. This may be attributed to the heat accumulation due to the multiple pulse irradiation, which increased the local temperature. This resulted in increased absorption along the incident laser path and prevented the delivery of a sufficient amount of energy to induce ablation on the back surface. The morphologies observed in the altered back surface were a granular band and a laser-induced periodic surface structures (LIPSS). Given that the etch rate of the back surface would be higher, wet etching was performed using an aqueous KOH solution. The 40% KOH solution was maintained in contact with the Si back surface at 25^0C while the laser was irradiated from the front surface. The laser beam was focused on the back surface and linearly scanned under different conditions. Focusing the laser approximately 15 μm into the liquid yielded deeper grooves as compared to those when it was focused precisely on the Si back surface. Further, the etch rate was

significantly higher compared to that during dry etching. I could achieve the maximum etch depth of approximately 6 μm during the wet etching process, in contrast to 0.3 μm during dry etching. However, the groove depth was not constant along the processing path. The morphologies observed in the altered back surface were different from those observed after dry etching. The results demonstrate a possibility of a new, efficient, and debris-free microfabrication technique.

I. Introduction

1.1. Background information

Si is a semi-conductor material widely utilized in a variety of applications in the modern era such as electronic devices, photovoltaic applications, and microelectromechanical systems (MEMS) [1, 2, 3]. Because of low production cost, integrated circuits are used in all electronic equipment today. Due to ability to endure a higher temperature, Si is better than germanium for being the material in integrated circuits. Si is the most commonly used material to create MEMS. Si becomes attractive for a wide variety of MEMS applications because of the economy of scale, high availability, low price and ability to incorporate with electronic functionality. Highly pure silicon wafers are used to make crystalline silicon photovoltaics, which are used to convert the sunlight into electrical energy. The need of the photovoltaics market is driven by increasing demand of electricity and renewable energy. Si is one of the most widely used material in photovoltaic technology to manufacture solar cells. In recent years, the demand of such elements is increasingly expanding so the demand for micro-processing technology of Si is growing.

However, there are many difficulties in conventional Si processing method. The most commonly used method to machine the Si is lithography technique, which requires many complicated steps and chemicals, causing heavy impacts on the environment. Moreover, it is difficult to meet the machining requirements due to low efficiency and precision. Other technologies include electrical discharge machining and laser machining [4, 5]. The laser machining has many advantages: avoiding the negative effects of tool wear, breakage, and mechanical stress; ensuring high machining quality and precision. When a long pulse laser acts on the material, it corresponds to the thermal ablation process. Recast layer and surface

cracks, which limits the improvement of machining quality, are caused by melting and vaporization.

Researchers pointed out that lasers with ultra-short pulse durations in the femtosecond to a few picosecond ranges provide a significant improvement in quality for processing various materials compared with nanosecond or longer laser pulses [6-10]. Since the high peak power can generate strong nonlinear effects inside the transparent medium, the short pulse width can effectively reduce the formation of the heat affected zone [11]. As a result of this, the ultrashort timescale and ultrahigh laser intensity induce nonlinear absorption right at the focus point, resulting in highly localized material ablation or modification with minimized mechanical and thermal damage of the ablated area. Therefore, ultra-short pulse machining can achieve high-precision and cleanliness without thermal stress and micro-cracks. In contrast, longer (nanosecond) duration pulses irradiated on the materials leads to continuous~~ly~~ heating of the target materials. Several researchers have attempted 3D micromachining on the surface or the interior of transparent dielectric materials by utilizing ultrafast lasers [12, 13, 14]. Applications of this method are based on laser-induced changes in the refractive index, which can be both positive and negative compared with unmodified materials. In addition to dielectrics, the formation of laser-induced subsurface modifications may have significance in the machining of Si [15]. As Si is the most popular material used in the production of integrated circuits, this technique may allow electronics and optical components to be integrated on a single chip.

Researchers used laser induced backside dry etching for laser patterning. Stone et. al [16] kept the glass substrate close to a graphite plate, then used the plate for laser patterning on glass. The glass substrate was in close contact with the graphite plate pressed by external force. At first, pulsed laser irradiation ablated the graphite plate. Under the effect of local high

temperature and high pressure, the graphite particles were separated from the graphite surface quickly, contacted with the melting glass surface, and combined with the surface of the glass, forming a black pattern. Laser patterning is applied for many purposes, such as bar codes. Moreover, the subtractive processing on Si backside can create 3D microfluidic structures in microchips or faulty isolation of IC chip package. [17]

Si is a semiconductor with a band gap energy of 1.12 eV, which corresponds to a wavelength of 1,127 nm [18]. Thus, an Si is considered as a transparent material for radiations longer than such wavelength. Consequently, the utilization of IR wavelengths longer than 1,127 nm would provide similar access to the interior of Si for laser-matter interactions as in transparent materials. Recently, researchers have attempted to modify the Si interior using ultrashort pulsed lasers at IR wavelengths. The laser pulses were focused in the interior of an Si substrate and the part near the focus position was modified. Various processing conditions have been investigated to understand the formation of modifications in the interior of Si [19-24]. However, using femtosecond lasers at wavelengths of 1,200 and 1,300 nm did not yield any modification [19, 20], even when multiple pulses with energies up to 90 μJ were applied [19]. Meanwhile, Verburg et al. demonstrated that modifications could be produced inside crystalline Si by a fiber laser, operating at the relatively long pulse duration of 3.5 ns and wavelength of 1,549 nm [21]. The refractive index of the modified portion of the Si crystal was also altered, and Pavlov et al. indicated that the modified parts demonstrated a waveguide action at the IR wavelength [22]. Kammer et al. [23] reported modifications in Si by a 1,552 nm wavelength laser with different pulse durations, ranging from 800 fs to 10 ps. They primarily focused on inscribing waveguides in the Si and describing the resulting internal modifications rather than examining the Si back-surface processing [22, 24]. Even most

previous research on laser-material interaction tends to highlight laser beam parameters and experimental setups for precision material processing, there is little emphasis on the optimal laser parameters to apply in laser material processing.

1.2. Objectives

Ito et al. demonstrated the machining of Si by passing a femtosecond laser of 1,552.5-nm wavelength through an Si substrate [25]. Previous research demonstrated that when the laser was focused on an Au film on the surface of a second substrate placed at the back of the first Si substrate, the Au film was ablated by irradiation through the Si substrate [26, 27]. Additionally, when the focus was placed at the back surface of the Si substrate and the aberration of the laser light caused by the large refractive index of Si was compensated for, the Au film on the back surface was ablated and deposited onto another substrate placed at the back of the substrate. Therefore, it would be possible to machine the back surface or the interior of Si by irradiating the focused laser through the substrate itself.

The purpose of this study is to examine the issues and challenges associated with 3D microprocessing on the back surface of Si using an ultrafast laser with a pulse width of 900 fs and wavelength of 1,552.5 nm. I attempted to create grooves, the simplest surface structure, on the back surface of an Si substrate and observed the peculiar behavior of the laser action in the interior and on the back surface of the substrate. I built a processing system, which can perform experiments while observing the focus position by combining infrared femtosecond laser and the infrared microscope with a correction collar on the objective lens. The correction collar was able to compensate high refractive indices of Si, which vary with wavelengths of laser and observation, and allowed to adjust the focus position in and through the Si precisely. Ablation processing the back surface and inside Si substrate will be carried out, as well as laser

assisted wet etching using KOH solution. The effects of the laser repetition rate, scan speed, and focus position were explored in detail.

II. Principle of laser processing relevant to this work

2.1. Laser ablation

Laser ablation is a process of removing layers from a solid by irradiating the surface with a pulsed laser beam laser [28]. It is one of the most common techniques to process materials. Laser ablation can be applied to create extremely deep and small holes through very hard materials such as diamonds or metals. It can also be used to determine the presence of a particular material on a surface. The CW laser produces a continuous, uninterrupted beam of light while the pulsed laser refers to a short time (e.g., nanoseconds to femtoseconds) output. With the same average output power, the peak power of a pulsed laser beam is much higher than that of a CW laser beam. Usually, laser ablation refers to removing material with a pulsed laser, but it is possible to ablate material with a continuous wave laser beam if the laser intensity is high enough. If laser intensity becomes larger than threshold value, at the solid surface the laser energy will be converted into thermal, photochemical and mechanical energy. As a result, neutral atoms, molecules, positive and negative ions, radical, cluster, electronic and light (photons) are released explosively then the surface can be etched.

When light reach of a material's surface, due to the discontinuity in the real index of refraction, a part of it will be reflected from the interface and the rest will be transmitted into the material. The fraction of the incident power that is reflected from the surface depends on the incidence angle and polarization of the light as well as the index of refraction of the material and the atmosphere [29]. Collisional absorption occurs when laser photon energy is transferred to the plasma (mostly) through the ion-electron collision [30]. From a classical viewpoint, the electron oscillates in the electric field of the laser beam. If no collision occurs, the electron continues to oscillate in phase with the electric field and gains no thermal energy. If there is a

collision with a nucleus, the oscillation energy of the electron is converted to random thermal energy. When a solid surface is irradiated by a long-pulsed laser beam, the material is heated by the absorbed laser energy. The thermal motion of some particles is accelerated. Once the absorbed energy exceeds the sublimation energy, these particles sublimate or evaporate and become vaporized particles.

Inside of a material, absorption causes the intensity of incident light to decay with depth at a rate determined by the material's absorption coefficient α [30]. In general, absorption coefficient is a function of wavelength and temperature, but for constant absorption coefficient, intensity I decays exponentially with depth *x* according to the Beer–Lambert law where I_0 is the intensity just inside the surface after considering reflection loss. As shown in Fig. 2.1 the light absorption in solid occurs at effective distance α^{-1} (absorption length) from the surface. Therefore, how quickly electrons (conduction band) and holes (valence band) are generated in the time laser pulse width irradiated or to transfer the energy to the lattice system, the distance that electrons and holes diffuse in solid, and the heat generated from the diffusion needs to be considered.

However, because the diffusion coefficient of electron-hole pairs, optical absorption coefficient, thermal diffusivity, and the energy gap is strongly dependent on the temperature. The temperature rise caused by heat energy discharged from the electron-hole pairs, situation changes drastically. This is because the temperature of the surface layer of the solid increases rapidly at positive feedback. For example, absorption coefficient increases slightly with the temperature rise, then absorption length will be shortened. In general, when the temperature increases E_G decreases, then the diffusion of hole and electron pairs is suppressed. In addition, thermal diffusion coefficient declines with the increase in temperature. Therefore, the area

closer to the surface will be heated more during laser irradiation period. As a result, laser wavelength with short absorption depths can allow local modification of surface properties without altering the bulk of the material.

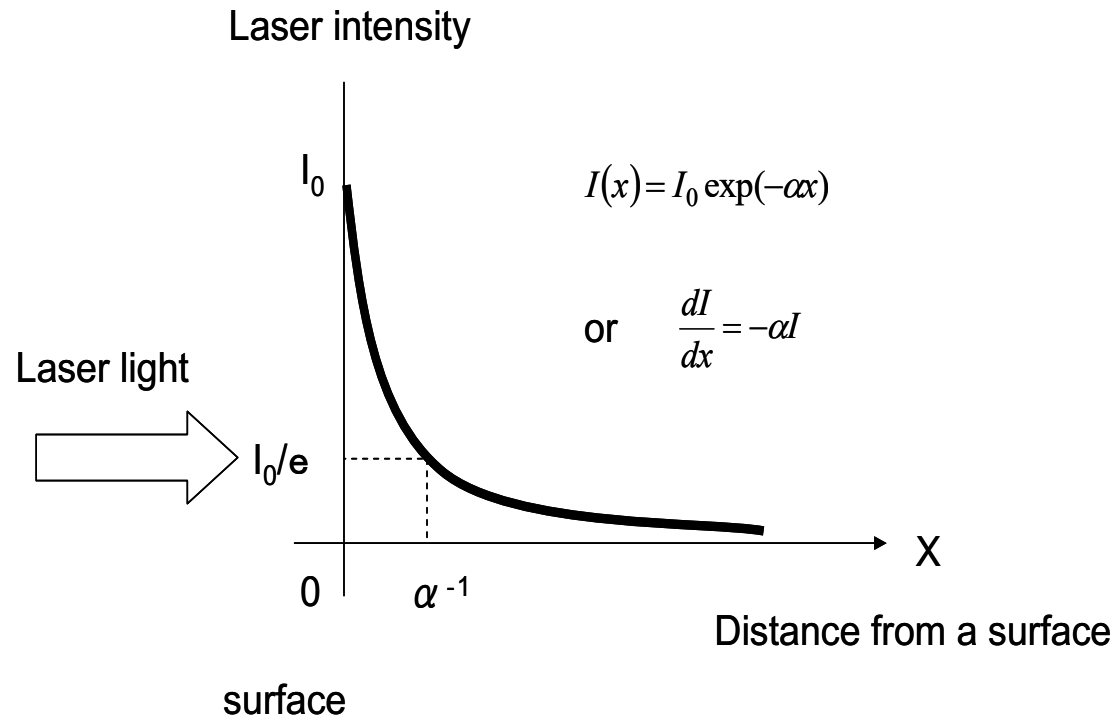

Fig. 2.1: Light Absorption Coefficient

2.2. Multi-photon absorption

Normally excitation occurs when a ground state electron absorbs a photon and jumps up to a higher, unstable energy level (Fig. 2.2 (a)). Multi-photon absorption is the simultaneous absorption of more than one photon of identical or different frequencies in order to excite a molecule from one state (usually the ground state) to a higher energy state. In the process of atom absorbing multiple photons, there is simultaneous multiphoton absorption (Fig. 2.2 (b)) and step-by-step absorption (Fig. 2.2 (c)). A typical nonlinear absorption process is two-photon absorption. Here, the energies of two photons are combined to excite a single electron into a higher state – e.g. above the band gap of a semiconductor. Thus, there can be absorption (at

high enough intensities) even when the energy of a single photon is insufficient for getting across the band gap. The effective absorption coefficient is proportional to the optical intensity. Similarly, there are multiphoton absorption processes involving more than two photons per process.

After the electrons absorb the energy, there will have thermalization at the end of the laser pulse. For a short-pulsed laser, the laser-material interaction time is short in comparison with atomic relaxation processes [28]. Therefore, the irradiated zone of the material quickly reaches vaporization temperature and the ablated particles evaporate from the surface. The duration time of the pulse is much less than the time taken by electrons, atoms, and excited molecules, to release heat energy by moving motion, which is too short for linear absorption processes such as the electron–phonon interaction process, single-photon process, and thermal diffusion process to happen. In consequence, nonlinear absorption process occurs during short-pulsed laser ablation.

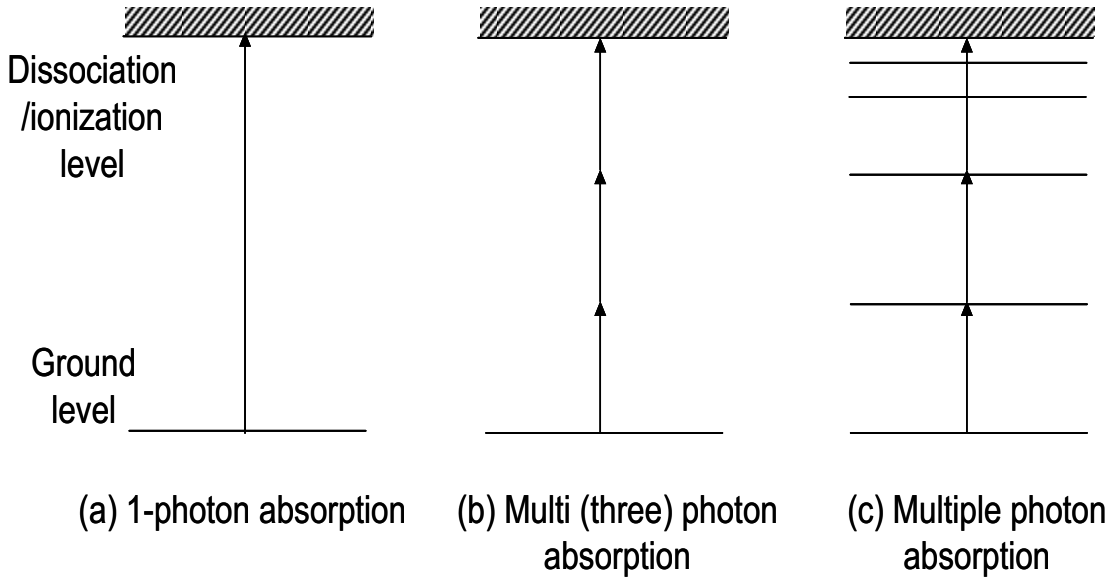

Fig. 2.2: Multi-Photon Absorption Process

2.3. Semiconductor material as transparent body

Generally, photons will couple into the vibrational or electronic states in the material depending on the photon energy. In semiconductors, the absorption of laser light mainly occurs through resonant excitations such as transitions of valence band electrons to the within bands (intersubband transitions) or conduction band (interband transitions) [31]. These excited electronic states can transfer energy to lattice phonons. If there is no impurity or defect states to couple to, energy below the material's band gap will not be absorbed. These energies typically correspond to light frequencies below the visible to infrared spectrum for semiconductors. The vicinity of the spectrum's absorption edge of Si and germanium is shown in Fig. 2.3. According to that graph, Si allows any light with the photon energy lower than 1.12 eV (wavelength larger than 1,127.3 nm) to transmit through. Further, Fig. 2.4 illustrates the transmittance of each wavelength for 300 μm thickness Si. If the wavelength is 1.24 μm or more, it can be seen that the transmittance is 51-52%.

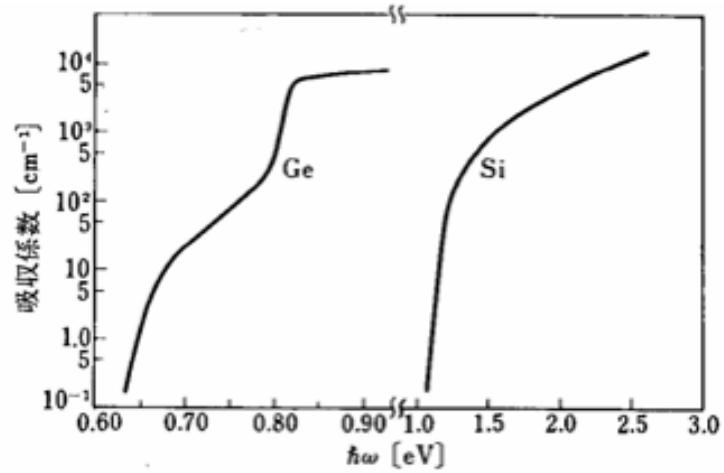

Fig. 2.3: The vicinity of the spectrum's absorption edge of Si and germanium

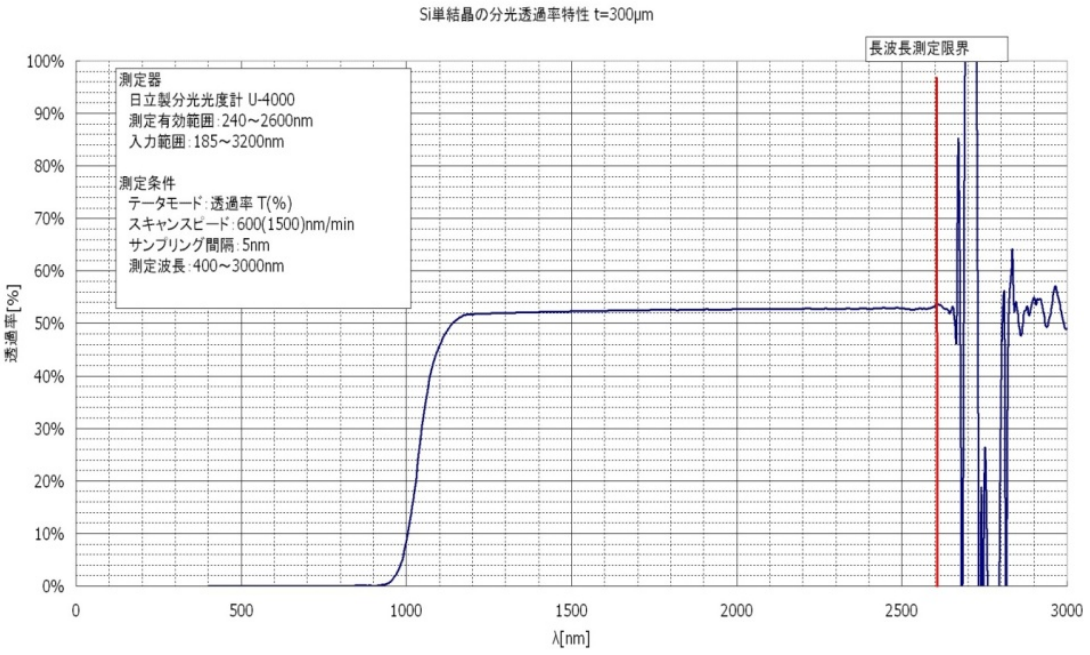

Fig. 2.4: The transmittance of wavelength for 300 μm thickness Si

2.4. Si ablation by femtosecond laser

With the same pulse energy, the laser's pulse width can have a significant effect on the dynamics of the ablation process. In general, as the pulse width is shortened, the peak power will increase [32]. The volume of material that is directly excited by the laser has less time to transfer energy to the surrounding material. Consequently, the ablated volume becomes more precisely, and the rest of the material has been less affected by the absorbed energy, which reduces the heat affected zones (HAZ) [33]. However, even for these ultrashort pulses, there is excess energy remaining in the material that can still cause thermal effects in the surrounding material after the pulse has ended.

In the ablation by femtosecond laser, laser energy absorbed in electronic system will transfer to the crystal lattice and ions in picoseconds. As a result, when the irradiation energy

is high enough, a high-density high-temperature plasma is generated, it causes a rapid expansion. During this time, the diffusion of heat to the irradiated area outside cannot be ignored, and is characterized by not undergoing liquefaction process caused by the intervention of normal nanosecond laser ablation. Therefore, efficient ablation can be performed with high accuracy. On the other hand, in the case of using a nanosecond order melt layer is formed around the irradiation region due to influence of the thermal diffusion is increased. In the case of processing the transparent optical material such as quartz or glass, thermal stress caused by the molten layer would thereby cause the cracking.

For opaque materials, optical absorption depths are very small. With femtosecond laser pulse width, the thermal diffusion length is relatively small. Therefore, I may consider during the initial interaction all of the optical energy as absorbed at the surface without significant thermal diffusion out of the irradiated region [19]. In addition, by increasing the absorption and diffusion lengths through the appropriate choice of laser wavelength this confinement can be relaxed. Consequently, in order to achieve the exact desired material outcome, it is very flexible in designing laser processes.

From these reasons, when treating the Si as a transparent material, it can be said that infrared femtosecond laser is suitable for the microfabrication.

III. Sample and experimental equipment

3.1. Laser System Schematic

The schematic diagram of the laser irradiation system is illustrated in Fig. 3.1. The laser pulses were steered by two mirrors and transferred to an IR microscope through its side arm. A visible-IR camera (Artray ARTCAM-130MI-HDM-NIR) was installed along the optical observation axis. This setup facilitated the simultaneous laser irradiation and observation of the back surface of Si by the IR camera. Inside the microscope system, a dichroic mirror, which reflects the processing laser light of 1,552.5 nm and transmits light in the range of 700-1,200 nm, was installed. For the IR observation, I used a filter to observe the Si sample using 1,100 nm light. An objective lens (x100, N.A. 0.85) equipped with a correction collar was used to minimize the aberrations caused by the high refractive index of Si, which is 3.47 at 1,552.5 nm [33]. To scan the laser, the sample was moved by an electric x-y stage ALS-602-H0M (Chuo Precision Industrial Co., Ltd.) with accuracy of 1 μm.

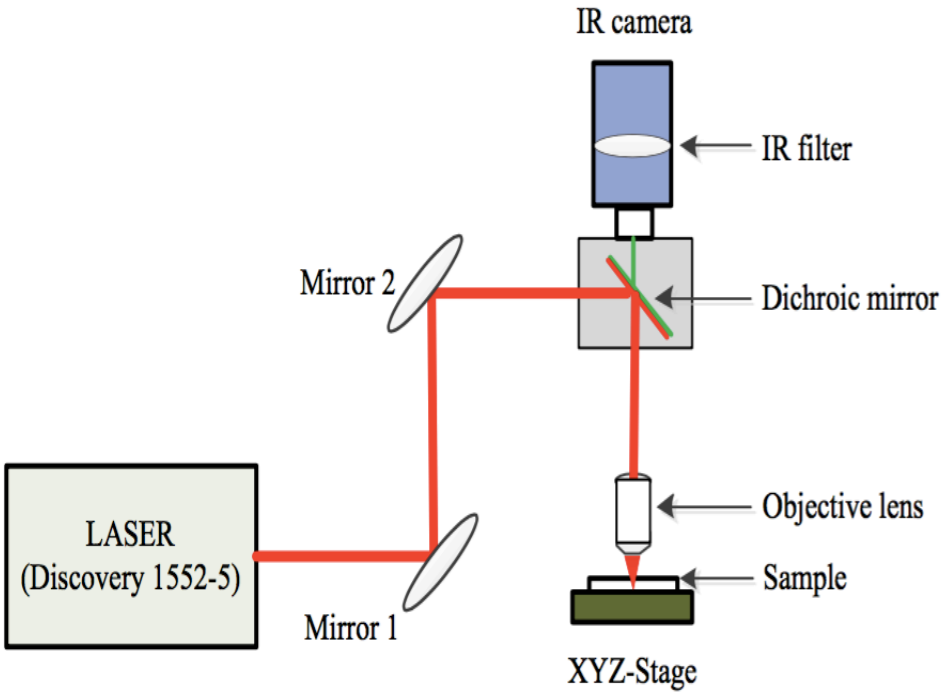

Fig. 3.1: Schematic diagram of experimental set up

3.2. Laser equipment

Table 3.1 illustrates the specifications of the fiber laser. An IR femtosecond fiber laser with a pulse width of 900 fs at a central wavelength of 1,552.5 nm was used in this study (Raydiance Discovery 1552-5). It could operate at an adjustable repetition rate *f* of 1 Hz to 500 kHz and an adjustable pulse energy of 1-5 µJ. Fig. 3.2 shows the beam profile of Discovery 1552-5; beam mode is Gaussian.

Center wavelength	1,552.5 nm
Pulse duration (FWHM)	900 fs
Repetition rate	1 Hz – 500 kHz
Energy per pulse	1 µJ - 5 µJ
Average power (max)	2.5 W
Beam diameter at output window	5 mm × 5 mm
Beam divergence	1 m rad

Table 3.1: Laser equipment specifications Discovery 1552-5

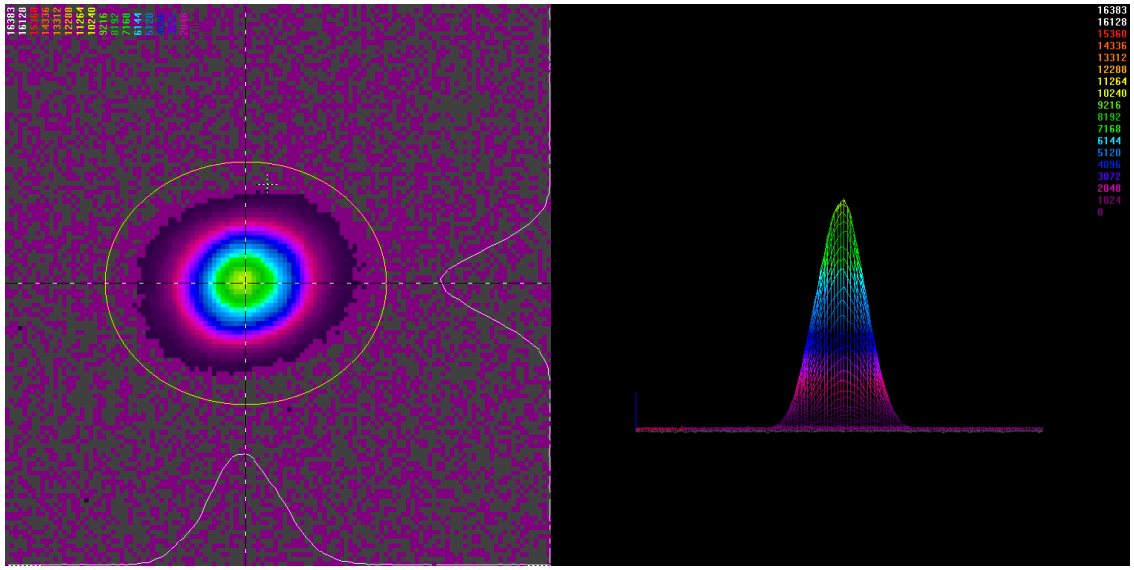

Fig. 3.2: Discovery 1552-5 Beam profile

3.3. Infrared camera

An infrared camera (Artray ARTCAM-130MI-HDM-NIR) was used to observe the sample during the experiment. The camera's quantum efficiency is shown in Fig. 3.3. The infrared transmission filter R70 (Hoya) is attached to the camera. The transmittance related to the wavelength is displayed in Fig. 3.4.

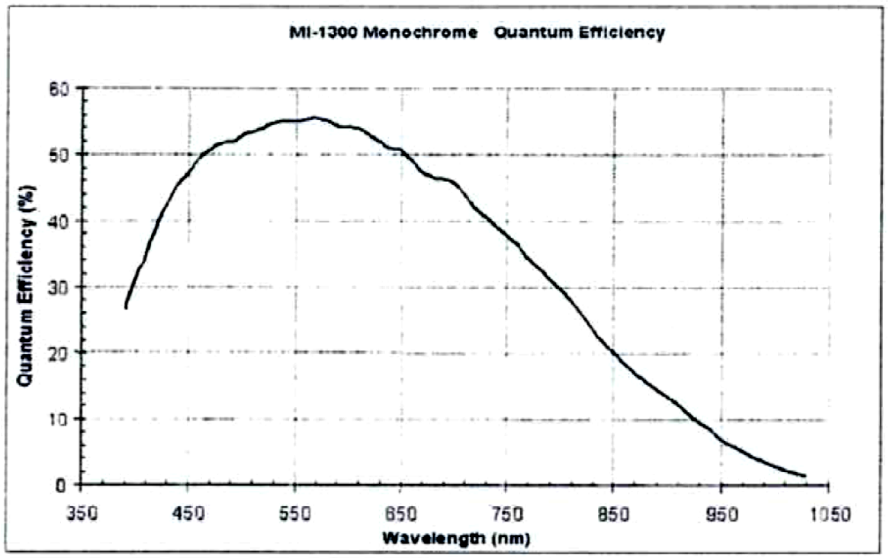

Fig.3.3: Infrared camera's Quantum Efficiency

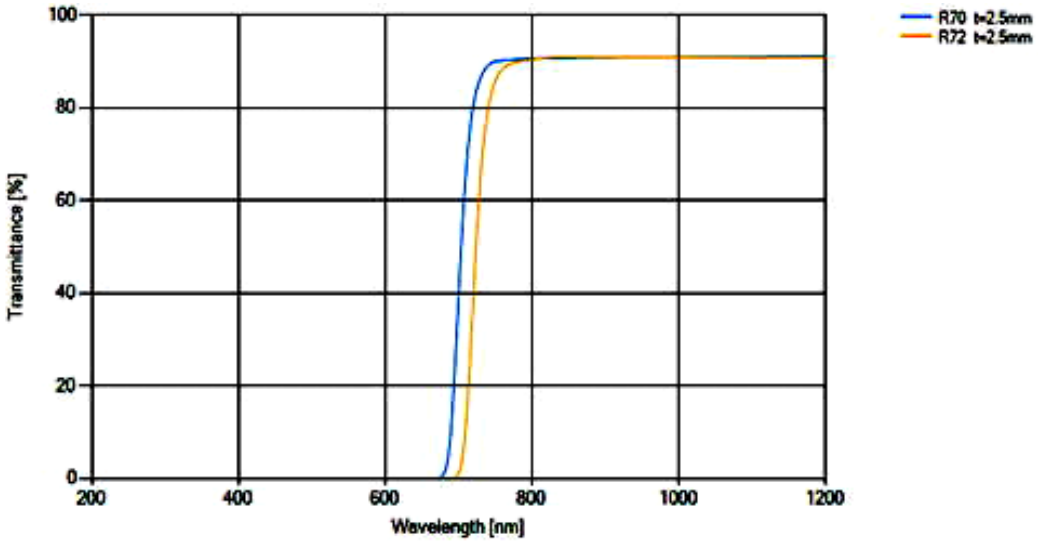

Fig. 3.4: Infrared filter transmittance related to wavelength

3.4. Objective lens

I used an infrared objective lens LCPLN100XIR equipped with a correction collar to minimize aberration. Fig. 3.5 shows transmittance related to the wavelength. Owing to the size of the laser beam and the acceptance diameter of the microscope as well as other losses, the measured energy of the laser pulses emitted from the objective lens was approximately one-fifth of that at the exit of the laser. In this study, I maintained the laser pulse energy at 4 μJ, which reduced to approximately 0.8 μJ after the objective lens. The spot size is shown in Fig. 3.6. The spot size was estimated by measuring the processing after focusing the laser directly on the Si surface then performing single sport irradiation. At this time, focusing the light above the sample surface is defined as plus, focusing the light within the sample is defined as minus. Spot size measured by this method was 3.4 μm.

Numerical aperture	0.85
Magnification	×100
Si aberration correction	0 mm~1.0 mm
Working distance	1.2 mm
Focus length	1.8 mm

Table 3.2: LCPLN100XIRS Specifications

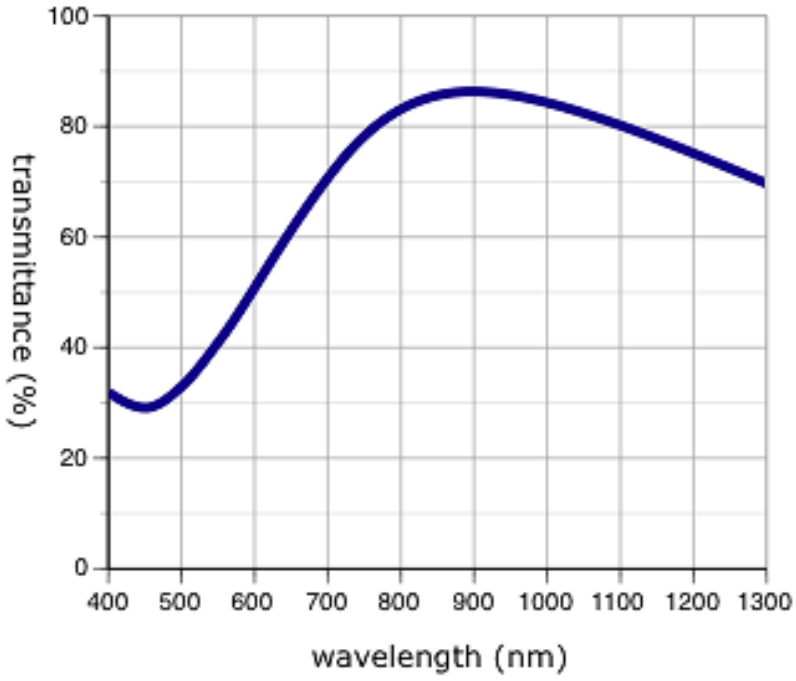

Fig.3.5: LCPLN100XIR Transmittance wavelength

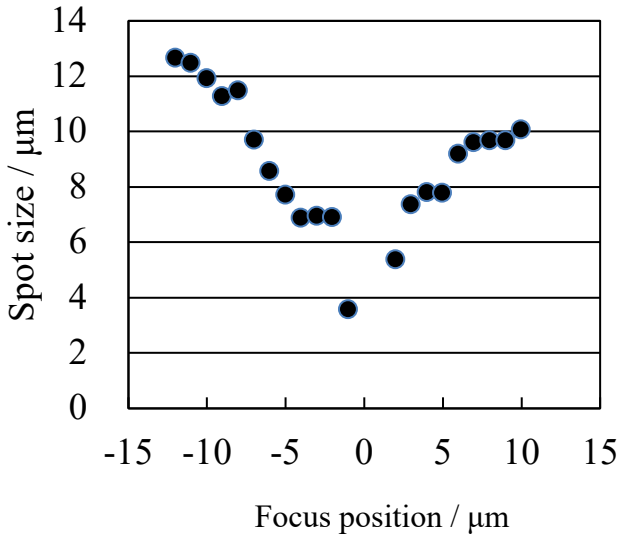

Fig. 3.6: Estimation of spot size

3.5. Electric stage

Scanning of the laser is carried out by relatively moving the sample using a motorized stage. Electric stage using is the ALS-602-H0M, a product of Chuo Precision Industrial Co., Ltd., and is applied in the operation of the Y-axis direction. Specifications of the stage are summarized in Table 3.3.

Resolution	0.001 mm
Lead screw	0.5 mm
Positioning accuracy	±0.02 mm
Repeat accuracy	±0.0005 mm
Motor used	PMM33BH2 equivalent (5-wire Pentagon connection)

Table 3.3: Motorized stage specifications

3.6. Sample

Surface properties	Both sides polished
Conductivity	P-type
Thickness	320±25 μm
Gravity (18ºC)	2.33g・cm^{-3}
Crystal orientation	100±2°
Resistivity	0.1～100 Ωcm
Melting point	1410 °C
Boiling point	2600 °C
Heat (27ºC)	0.716 J/g・K
Thermal conductivity	168 W/m・K
Thermal expansion coefficient (300ºC)	4.2×10^{-6}
Band gap	1.12 eV
Refractive index (wavelength 1120 nm)	3.5316
Refractive index (wavelength 1152 nm)	3.4784

Table 3.4: Si sample physical properties

A double-sided polished P-type Si wafer with a thickness of 320 μm and (100) crystal orientation was used in this research. The sample specifications are shown in Table 3.4. Samples used have thickness 320 μm. Band gap of the Si substrate is 1.12 eV. At a wavelength of 1,120 nm, refractive index is 3.5316, and at 1,552.5 nm, it is 3.4784 [34, 35].

3.7. Observation and analysis of the sample

- Observation of sample surface and internal modification: The optical microscope used to observe the sample was the same to the infrared microscope used for processing. An infrared filter which blocks visible light was attached to the microscope. By the filter, it was possible to switch between the observation with the visible light and the observation with only the infrared light. By observing with infrared light, it was possible to observe Si as transparent material.
- A scanning electron microscope (SEM) and a Raman spectroscopy (Jasco NSR-7200) was implemented to study the crystal structure of Si.
- A laser microscope (KEYENCE VK-8710) was implemented to measure the depth of processed lines on the Si back surface.

3.8. Defining the focus position

The focus of the objective lens on the back surface of the substrate was denoted as the focus position (± 0 μm). To set this focus position, I created markings by scanning the focused laser beam directly on the front surface to generate a pattern shown in Fig. 3.7 before machining the substrates. The lines formed were continuous grooves of 16 μm width and 3 μm depth. Then, the Si substrate was rotated and the markings now on the back surface were observed by IR light. When the clearest image of the markings was obtained by adjusting the lens position and correction collar, it was considered that the 0 μm focus position was set. I

performed the observations at three different positions illustrated in the left panel of Fig. 3.7 and set them at the same focus position as shown in the right panel of the figure. With this technique, the change in the focus position during the laser scan was minimized. The movement of the focus position toward the front surface of the Si substrate, i.e., in its interior, was expressed as positive values in μm, while positions in the opposite direction from the 0 μm focus position were expressed as negative values. Laser scanning was performed after adjusting the focus position appropriately.

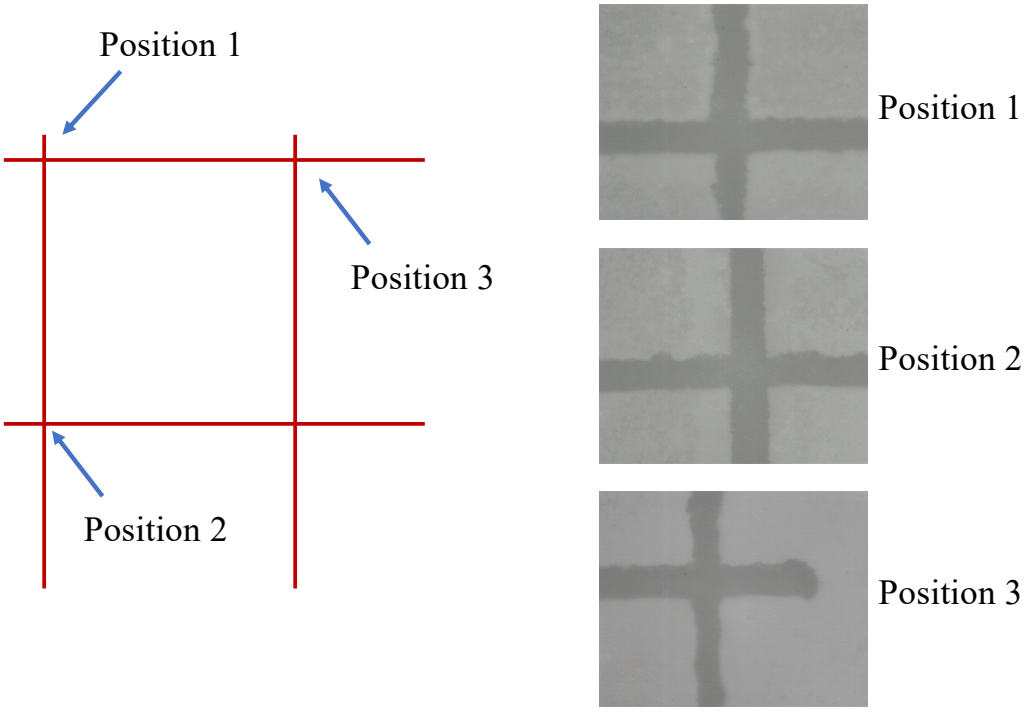

Fig. 3.7: Pattern of markings on the Si back surface, formed by direct irradiation of the laser (left), and sample IR micrographs of the cross points of the markings (right).

3.9. Thickness of Si and correction collar of objective lens

The appearance of the objective lens used is shown in Fig. 3.8. The objective lens used in the experiment is possible to correct aberrations based on Si thickness by adjusting the value of the correction collar. For light having wavelength of 1,100 nm ~ 1,300 nm, the correction value can be set between 0 to 1.00, thus it is possible to correct the aberrations of 0mm ~ 1mm thickness Si. In addition, its resolution is up to 0.025 by putting the auxiliary scale. A cover glass with thickness of 0.15 mm is attached for the purpose of protecting objective lens. Correction value for the 0.15 mm thickness glass is 0.25. Therefore, correction value in this experiment is a value obtained by adding the correction value for the thickness of the Si to correction value for the thickness of the cover glass of 0.25. Correction values which are mentioned in this paper are referred to the values used in the actual experiment.

Fig. 3.8: Objective lens with correction collar

IV. Effect of correction value of objective lens on back surface processing

4.1. Experimental

In the case of observing the Si back surface with IR light, the observation image of the mark in the back surface has become the clearest when adjusting the-value of the correction collar at 0.575. Thus, when observing the mark in the back surface, the correction value is fixed at 0.575, then I examined the effect of focus position on the Si back surface processing. The laser of f = 500 kHz was scanned linearly at a scan speed of v = 400 μm/s. In this condition, there was about 4200 pulses on one irradiating spot, i.e., overlap rate was 99.9%. The laser was irradiated from front surface of the Si substrate, then, the processed part was formed on the back surface by focusing the laser on the back surface. Figure 4.1 showed the microscopy images of the Si front surface (top) and back surface (below) observed with IR light and visible light after laser scan with v = 400 μm/s at f = 500 kHz with different focus position. The laser scans started from the left side of the sample; the focus position moved in the positive direction in progresses to the right. From the front surface, machined traces could be observed by only infrared light when focus position located in the vicinity of ± 0μm. On the other hand, in the observation from the back surface, even by visible light, machined traces could be seen when focus position was in the vicinity of ± 0μm. When the focus position was close to the back surface, no change happened in the incident surface of the laser. It is understood that it is able to process on only the back surface by transmitting the laser through the Si substrate. In addition, the processed lines that appeared when focus position was 50 μm or more was the result of front surface processing since the focus position is near front surface. There was no

position at which the lines in the front surface and the back one overlapped. It can be concluded that based on this system, it was possible to do the selective processing by changing focus position.

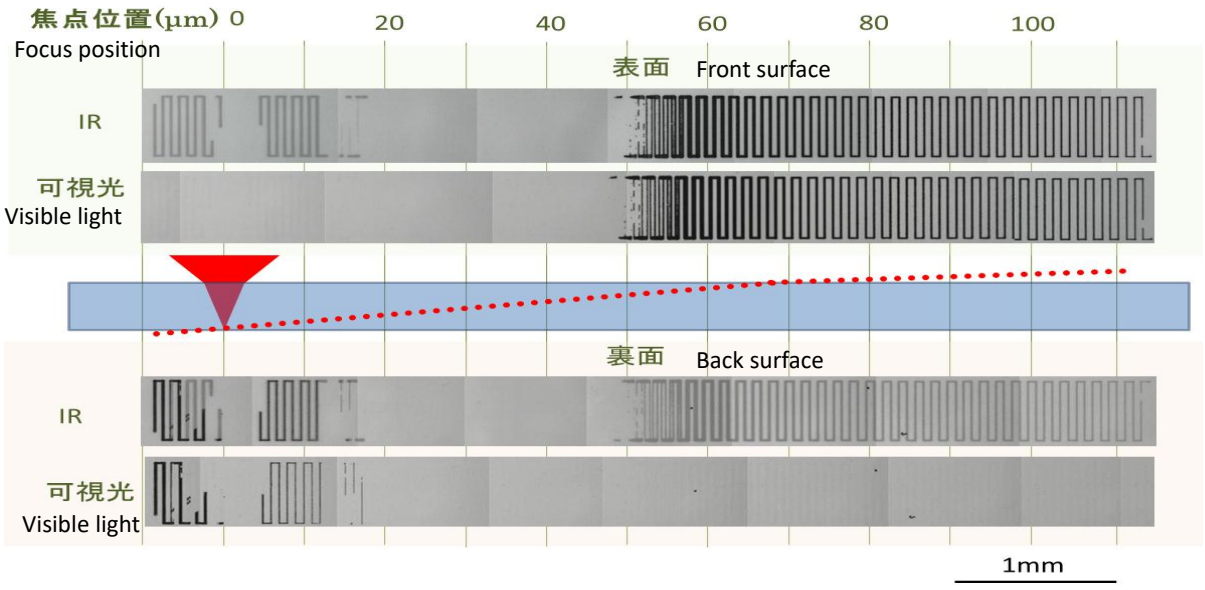

Fig. 4.1: Microscopy images of the Si front surface (2 above figures) and back surface (2 below figures) observed with IR light and visible light after laser scan with v = 400 μm/s at f = 500 kHz with different focus position.

4.2. Observation of processing on Si back surface

Fig. 4.2 shows the laser irradiation results on the back surface while varying the focus position from -16 to +8 μm observed by infrared light and visible light. The repetition rate was 500 kHz, the scanning speed was 400 μm/s and the value of correction collar of the lens was 0.575. It is noteworthy that no noticeable change is observed on the front surfaces of the irradiated substrates in the optical, laser, or SEM observations. The figure is obtained by observing directly from the sample back surface. In the infrared observation, processed lines can be observed in a wider range from the focus position -15 μm to +7 μm with some parts in dark colour and the other in faint colour. The dark colour parts observed in infrared light

correspond to the processed parts observed in visible light. When the focus position is ± 0μm vicinity, no change can be observed. On the other hand, in visible light observation, machining at the focus position -12 μm to -2 μm cannot be seen.

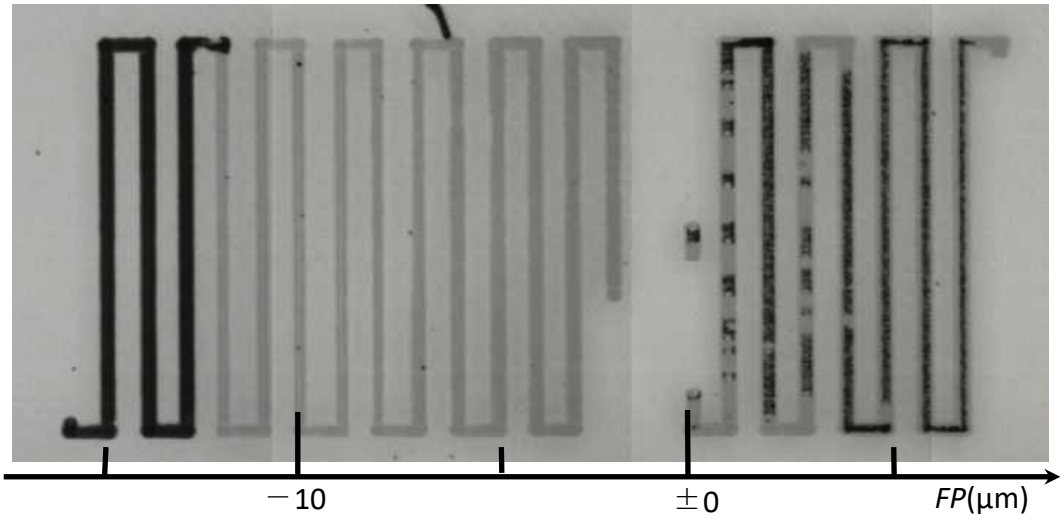

Observed with infrared light

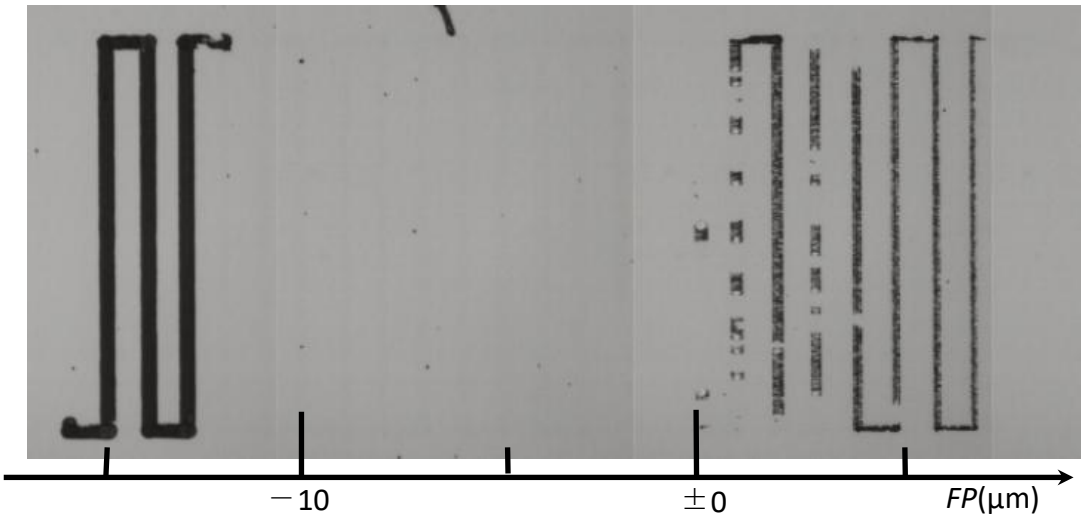

Observed with visible light

Fig. 4.2: Microscopy images of the back surface observed at (above) visible and (below) IR wavelengths after laser scan with v = 400 μm/s at f = 500 kHz. Scan length was 500 μm. 2 neighboring lines have focus position differ by 1 μm and 50 μm interval.

Fig. 4.3 shows the results of the SEM observation at the center of the processed lines when the focus position was -15 μm, -5 μm and 5 μm. At focus position -15 μm, a band of granular structure with particle size 500 nm was formed on the line width of 21 μm. Changes were not observed in Si back surface at focus position -5 μm. At the focus position 5 μm, structures similar to the focus position -15 μm was formed on the line width of 10 μm.

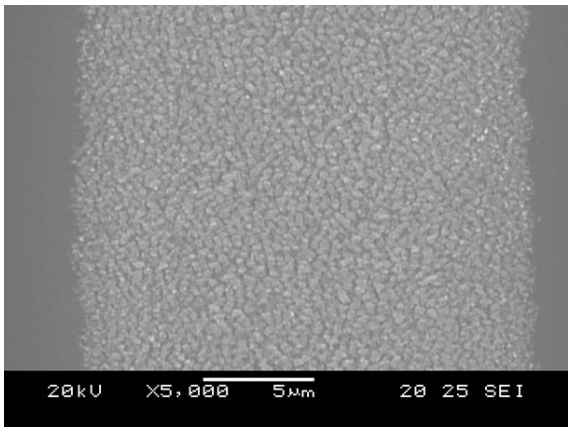

Focus position -15 μm

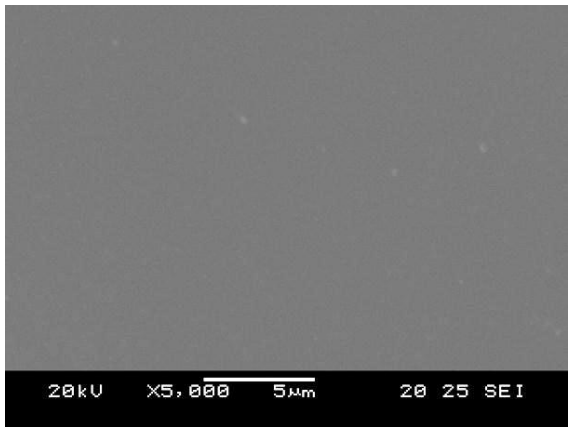

Focus position -5 μm

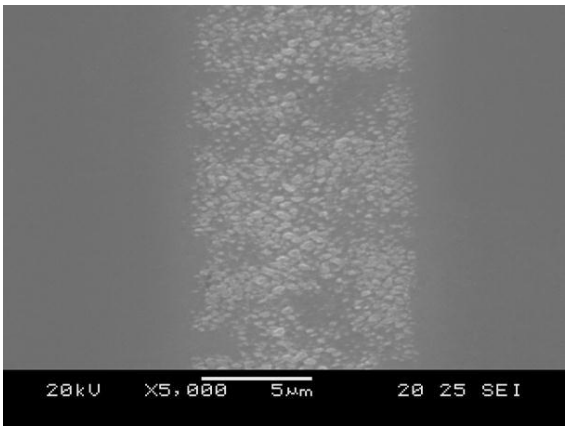

Focus position 5 μm

Fig. 4.3: SEM observation of the back surface after laser scan with v = 400 μm/s at f = 500 kHz. At the focus position-15 μm, granular structure with particle size 500 nm was formed on the line width of 21 μm. Changes were not observed in Si back surface at focus position -5 μm. At the focus position 5 μm, structures similar to the focus position -15 μm was formed on the line width of 10 μm.

4.3. Summary and discussion

When the collar was set at 0.575, and the laser was irradiated, it was found that:

- No change could be observed at focus position ± 0μm even by the infrared light.
- The structural changes in Si back surface had form of 500 nm size particles.

The reason why complex effects of laser irradiation were observed in this way was believed to be the difference in wavelength of the laser beam when performing processing and observation light (Fig. 4.4). Wavelength used for observation of the sample back surface was infrared light through a bandpass filter 1,100 nm, but the processing laser is an infrared laser with a wavelength of 1,552.5 nm. Because of the difference in refractive index due to the wavelength, there was deviation of the focus position after transmitting Si between processing and observation. In order to reduce aberration, it was necessary to do experiments with different values of the correction collar for observation and processing.

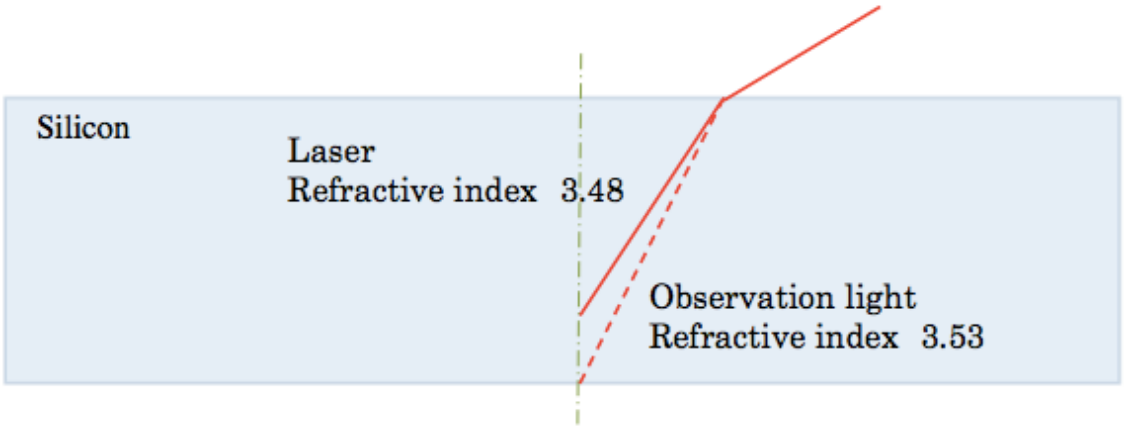

Fig. 4.4: Difference of Si refractive index for laser wavelength and observation light wavelength

The aberration correction for focusing the laser on the Si back surface differed from the aberration correction for observation. It is necessary to add a small readjustment to the

correction value. After observing the back surface marker by correction value 0.575 to determine the focus position ± 0 μm, the laser was scanned with different correction value. The laser of f = 500 kHz was scanned linearly at a scan speed of v = 400 μm/s. It was found that, if an appropriate value correction value was applied, aberrations should be minimized at the focus position ±0 μm. By far, the correction value 0.600 was believed to be the most suitable for Si back surface processing since it could process the Si back surface at the focus position ±0 μm rather than other correction value. Theoretically, if low correction value is applied, the appropriate ~~of~~ laser focus position tend to move to the back surface. Since correction value is lower, processing should occur on the back surface at the position of the negative focus position. However, the relationship between focus position at which processing occurs in the back surface and the correction value does not follow the theory. The reason for this is difference of aberration reduction and the correction value due to the movement of the focus position mutually influence each other, as well as the energy density on the back surface changed in a complex way.

Fig. 4.5 shows the observation of processing on the back surface after laser scan with v = 400 μm/s at f = 500 kHz while varying the focus position from -16 to +5 μm with the correction value 0.600. The above figure was obtained by using the visible light to observe while the below one was done by infrared light. The laser was scanned from the left side of the sample, the focus position was moved to the positive direction when progressing to the right. Under IR observation, the processing can be observed in the range of the focus position from -16 μm to +3 μm. At the focus position close to ± 0 μm (from -2 μm to +2 μm), the processing can be observed with the visible light. In the following laser scan, all the experiments were carried under correction value of correction collar 0.600.

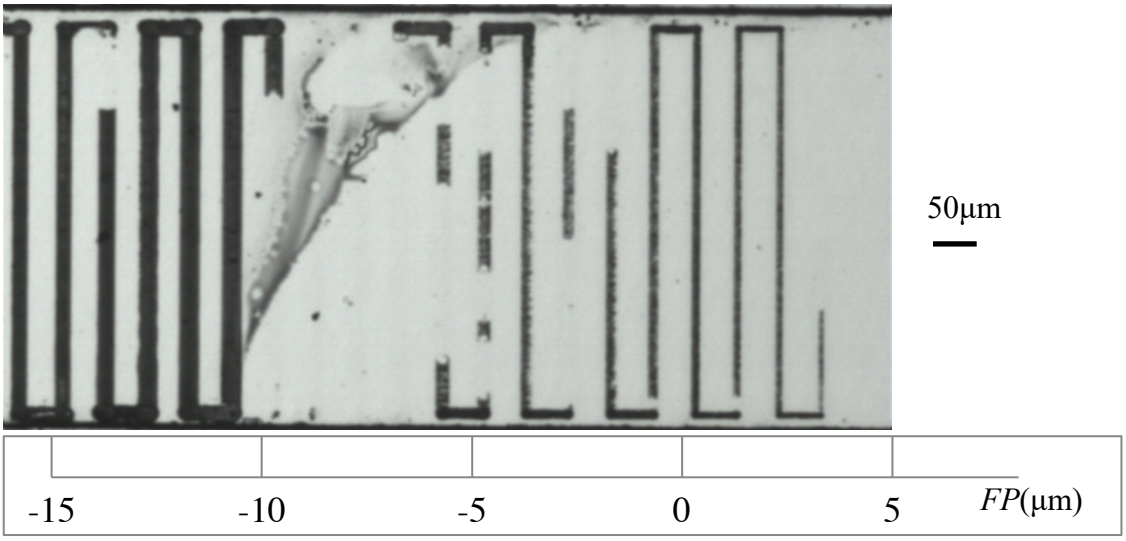

Observed with visible light

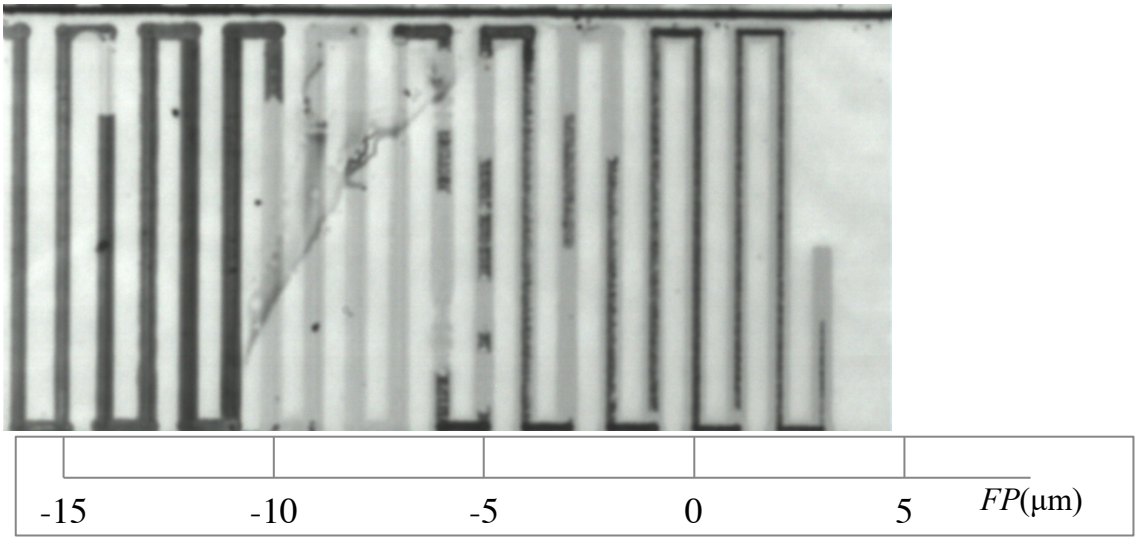

Observed with infrared light

Fig. 4.5: Microscopy images of the back surface observed at (above) visible and (below) IR wavelengths after laser scan with v = 400 μm/s at f = 500 kHz. Scan length was 500 μm. 2 neighboring lines have focus position differ by 1 μm and 50 μm interval.

V. Machining on Si back surface

5.1. Introduction

Following the previous research, I started to do the machining on Si back surface by irradiating the laser through the substrate with appropriate focus position and readjustment of the correction collar. The laser pulse energy was kept constant at 0.8 μJ. I tried to change the focus position, scanning speed and repetition rate to examine the effect of them on Si back surface machining. At first, single spot irradiation was performed then laser scanning followed later.

5.2. Experimental results

Firstly, several spot irradiations were performed by multiple laser pulses. Each spot was irradiated by 100,000 laser pulses with f = 500 kHz while the focus position was set at 0 μm. The distance between two consecutive spots was 50 μm. Microscopic observation of the back surface revealed dark spots at the irradiated positions, as shown in Fig. 5.1. The surface morphology of the dark spots consisted of many fine particles with a diameter of approximately 500 nm. However, these dark spots disappeared from several points, even though the laser irradiation conditions were unchanged. The short axis of the spots varied from 10-14 μm, whereas the long axis of the spots varied from 14-16 μm. The long axis of the spot corresponded to the laser polarization axis and was considered as the laser spot size. The non-circular shape of the spot could be due to the intensity distribution of the laser pulse, which might have been enhanced by the strong aberration in Si [18]. The fluctuation in the observed spot size as well as the instability of the spot appearance suggested that there would be a stochastic incubation effect in the nonlinear processes in Si under the laser irradiation conditions.

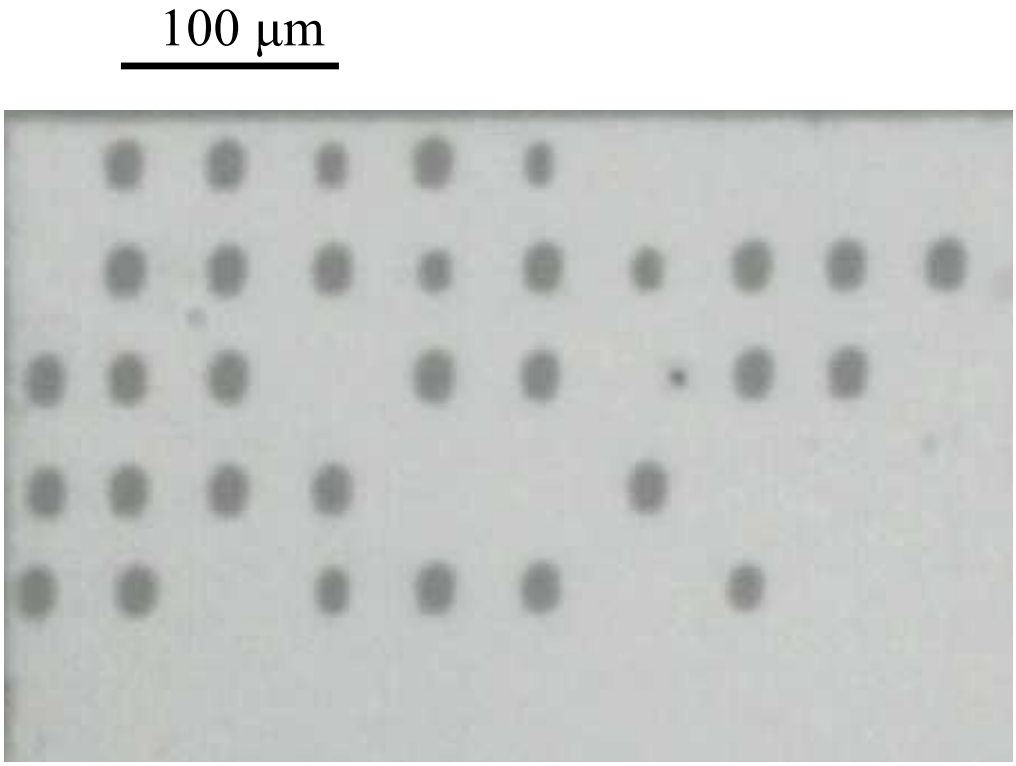

Fig. 5.1: Visible micrograph of the Si back surface after multiple shots irradiation on the same point at a focus position of 0 μm. Several dark gray spots appear at only some of the irradiated positions, even though the laser irradiation conditions are kept constant. The distance between two consecutive spots is 50 μm.

To realize the machining of grooves on the back surface, the laser of f = 500 kHz was scanned linearly at a scan speed of v = 20-800 μm/s. The focus position was set at 0 μm. Fig. 5.2 shows the microscopy images of the back surface observed at the (a) visible and (b) IR wavelengths, as well as the (c) scanning electron microscopy (SEM) image after the laser scan with v = 800, 400, 100, and 20 μm/s at f = 500 kHz. The scan length was 500 μm, and the scans were repeated twice in reverse directions for each v at a 50 μm interval. In the IR images, gray lines appeared along the scan line with scattered black sections, which corresponded to the changes observed with visible light or in the SEM images. In the visible and SEM images, changes corresponding to the gray lines observed in the IR images were not observed. This

indicated that the gray sections observed under IR light reflected the changes occurring in the interior of Si. When the laser was turned on and the scans were immediately started, the changes in Si, which were observed as gray lines or spots on the IR camera screen, were observed not instantaneously but only after certain scan lengths. This demonstrated that the incubation effect could occur during Si processing, as mentioned for the scattered results shown in Fig. 5.3. Ablation threshold fluence is defined as the minimum laser fluence necessary to initiate the ablation process. In the multi-pulse regime, it is well established that the ablation threshold depends on the number of laser pulses exciting the same spot. The threshold fluence is reduced with increase in the number of pulses exciting the same spot [36, 37]. However, the origin of this incubation is still under debate.

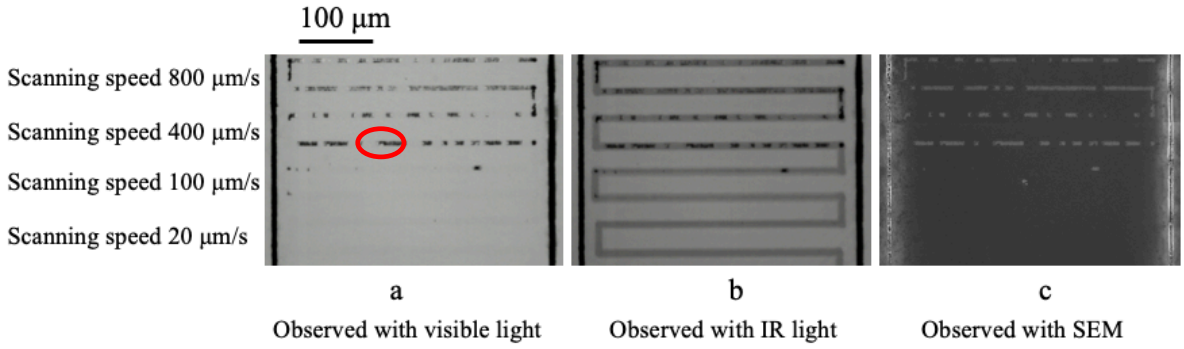

Fig. 5.2: Microscopy images of the back surface observed at (a) visible and (b) IR wavelengths as well as (c) SEM images after laser scan with v = 800, 400, 100, and 20 µm/s at f = 500 kHz. Scan length was 500 µm and scans were repeated two times for each v with a 50 µm interval in the reverse direction. The width of the gray lines (IR) was larger than that of the black lines (visible) observed at the same positions. In the IR image, gray lines appeared along the scan line with scattered black parts, which corresponded exactly to the changes observed with visible light or in the SEM images. The microscopy with visible wavelength and SEM images showed no changes corresponding to the gray lines observed in the IR images.

Although the incubation effects sometimes showed a rather scattered appearance, the laser irradiation could induce observable effects once the gray spots appeared at the beginning of irradiation. Therefore, the analysis in this study was restricted to the laser scans after the occurrence of the changes at the starting point of the scans. Although the incubation period that triggered such modifications varied from a few seconds to nearly a minute, I started the laser scan only if the processed spot was visible. The gray lines (changes or modifications in the interior of Si) occurred continuously whereas the black lines (changes on the back surface) appeared in a rather discrete manner, in which intermittent changes were observed. The width of the gray lines (IR) was approximately 12 μm for v = 800 μm/s and approximately 16 μm for other values of v such as 400 μm/s and 100 μm/s. Moreover, they were larger than the width of the black lines (visible) observed at the same positions, which was approximately 8 μm. The changes on the back surface appeared, then disappeared (as indicated by red circles in the figure), and then reappeared again. Even along a single line, some positions showed changes only in the interior of Si, whereas other positions displayed simultaneous changes on the back surface.

I changed the distances between the neighboring lines to explore whether or not the distance influenced the stability of the processing. From top to below of the figure 5.3, I scanned the laser with f = 500 kHz and v = 400 μm/s in the following order: 5 lines with distance 50 μm; 5 lines with distance 10 μm; 5 lines with distance 20 μm; 5 lines with distance 50 μm. Even when the distance between neighboring lines was 10 μm, which was less than the width of the lines observed with the IR light (the processed lines overlapped each other), the changes on the back surface did not continuously appear. To check whether the pre-processed area of the markings affected the stability or processability of the processed lines, I initiated

the scan at points far from the markings, which were inscribed in advance on the surface. I observed the Si back surface after laser scans at v = 400 μm/s and f = 500 kHz, starting at 510 μm from the vertical mark and 400 μm from the horizontal mark (Fig. 5.4). The distance between each line was 50 μm. The result was similar to those of the previous experiments: the lines observed with the IR light were continuous, whereas the lines observed with the visible light were intermittent. Therefore, there was no influence of prior machining of groove-mark on the processing stability on the back surface.

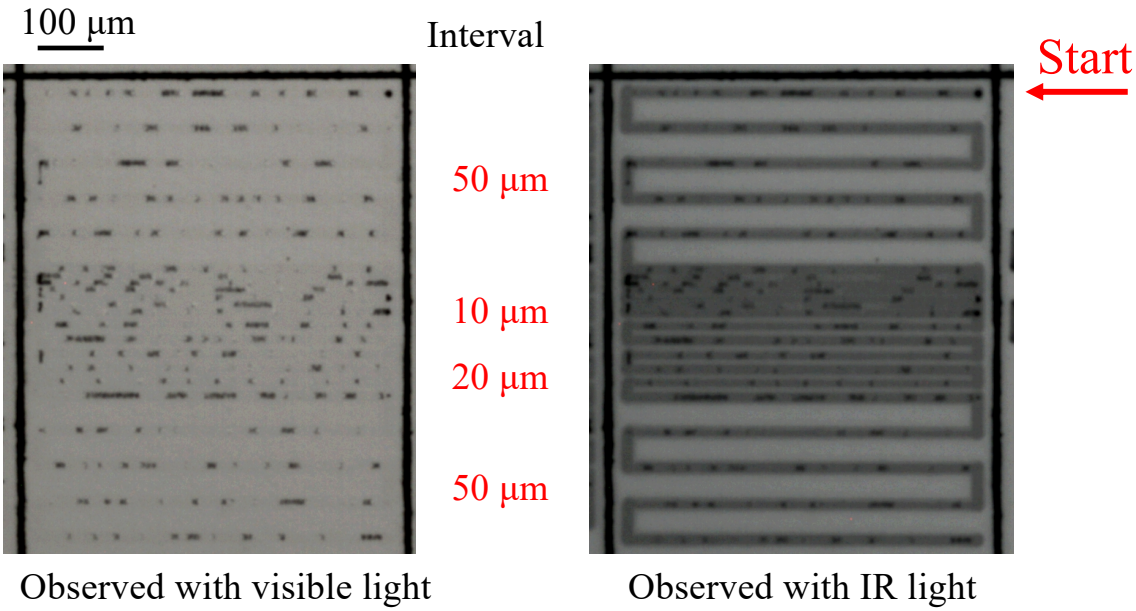

Fig. 5.3: The visible and IR observation of Si back surface after laser scan with f = 500 kHz and v = 400 μm/s with different intervals between neighboring lines. The changes in the interior of Si occurred continuously while the changes at the back surface occurred intermittently. The interval of neighbor lines shows no effects.

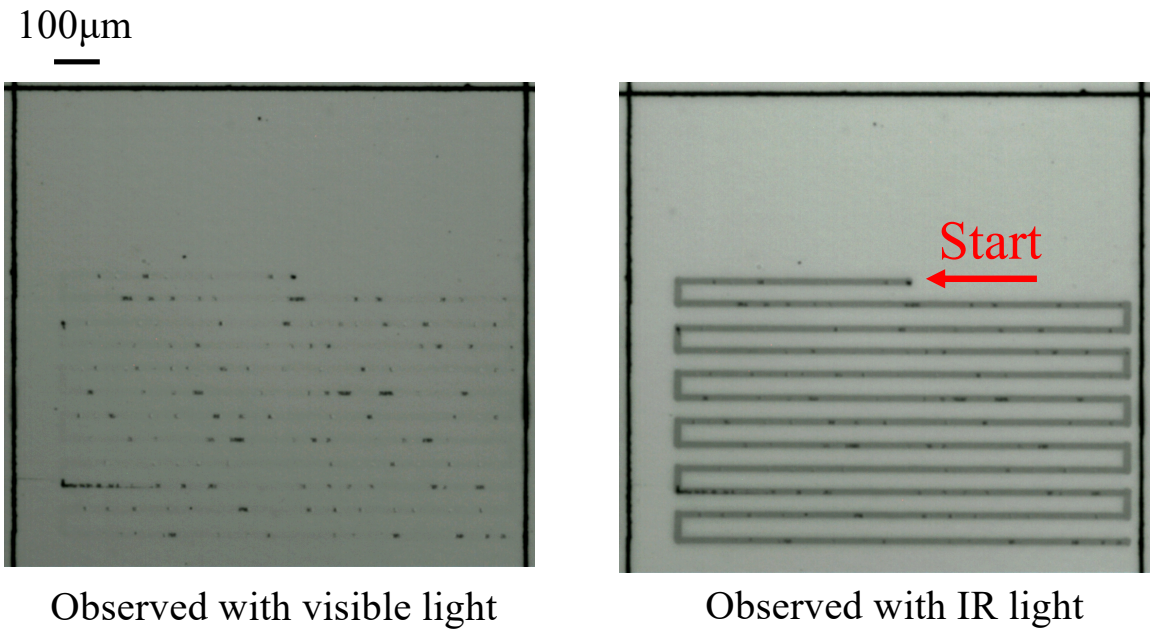

Fig. 5.4: The visible and IR observation of Si back surface after laser scan with f = 500 kHz and v = 400 μm/s when the distance of starting point was 510 μm from a vertical marker and 400 μm from a horizontal marker. The changes in the interior of Si occurred continuously while the changes at the back surface occurred intermittently.

SEM was utilized to observe the morphology changes on the back surface. Fig. 5.5 shows the morphologies on the back surface after laser scanning with f = 500 kHz and v = 100 μm/s. The processed lines consisted of non-processed areas as well as surface-modified areas with two characteristic morphologies: laser-induced periodic surface structure (LIPSS) and granular structures. The orientation of the LIPSS was parallel to that of the laser polarization, with a periodicity varying from 270-330 nm. The periodicity was estimated by measuring the sum of the distance between 6 consecutive parallel lines and then dividing by 5. LIPSSs on the surfaces of various substrates have been studied extensively; however, most of the LIPSSs reported thus far have been formed on the front surface of the substrates [38] , on the surface of the side wall on the machined structures [39], or inside transparent dielectrics [40]. Our previous report was the first to describe the formation of a LIPSS on the back surface of Si by

IR laser irradiation through the substrate [41]. The granular structures comprised round grains with approximately 500 nm diameter on the Si back surface. The three morphologies (LIPSS, granular structures, and unchanged morphology) seemed to appear in the order of LIPSS, granular, and unchanged morphology along the laser scan direction.

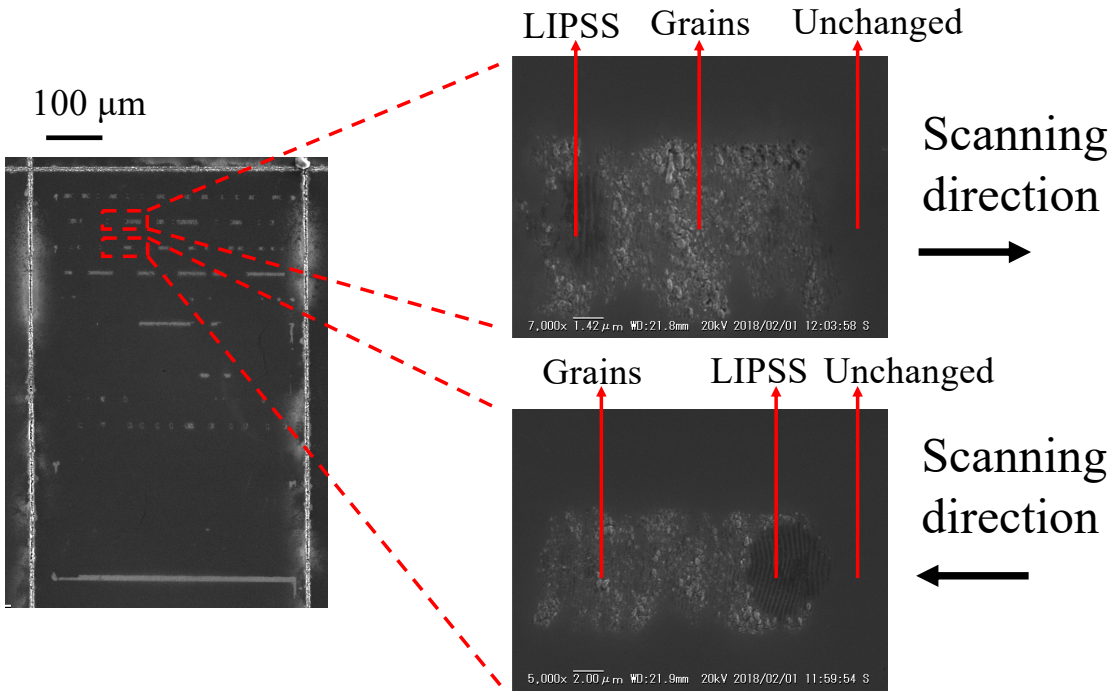

Fig. 5.5: SEM observation of Si back surface after laser scan with f = 500 kHz and v = 100 µm/s. Unprocessed parts and surface-modified parts existed along the processing lines, which had two characteristic morphologies: LIPSS and granular structures. The orientation of the LIPSS was parallel to the laser polarization with the periodicity varying from 270 to 330 nm. The morphologies appeared in the order of LIPSS, granular, and unchanged morphology along the laser scan direction.

5.3. Raman analysis of irradiated positions

Raman spectroscopy was implemented to investigate the structures of different zones observed after laser irradiation. Fig. 5.6 shows the Raman spectra of the Si back surface at 3 positions: (a) unirradiated position, (b) position where the changes occurred only in the interior of Si, and (c) position where the changes occurred on the Si back surface (c). At the unirradiated position of the substrate, the Raman spectrum was dominated by the signal at 530 cm^{-1}, which corresponds to crystalline Si. At the position where the processing occurred only in the interior of Si, there was one sharp peak at 530 cm^{-1} [42] , indicating no modification in the crystal structure on the surface compared with the structure of the unirradiated part. At the position where the changes appeared at the back surface, a broader band was observed at approximately 480 cm^{-1}, which is the characteristic peak of amorphous Si [43], was observed in addition to the peak at 530 cm^{-1}, in both the LIPSS and the granular structure. Therefore, the structural changes from crystal to amorphous Si were accompanied, at least partly, by morphology changes on the Si back surface.

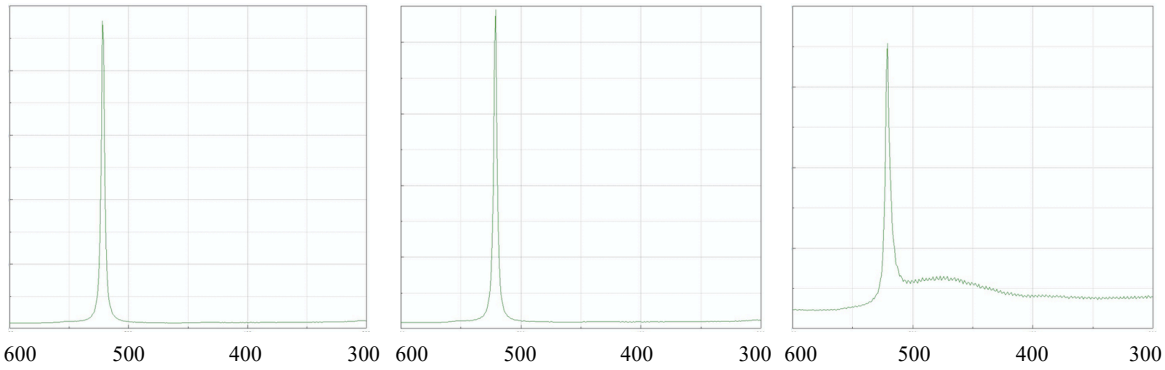

Fig. 5.6: Raman spectra of Si back surface at three positions: (a) unirradiated position, (b) position where changes occurred only in the interior of Si, and (c) position where the changes occurred on the Si back surface. At the unirradiated position, the Raman spectrum was dominated by the signal at 530 cm^{-1}. At the position where the processing occurred only in the interior of Si, there was one sharp peak at 530 cm^{-1}. At the position where the changes occurred at the back surface, a broader band at approximately 480 cm^{-1} was observed in addition to the peak at 530 cm^{-1}.granular, and unchanged morphology along the laser scan direction.

5.4. Cross-sectional observations

The Si substrate was cut perpendicular to the scan direction, and the cross-sections of the laser-irradiated positions were scrutinized. First, the substrate was cut across the scanned line at its center and then fixed by epoxy resin. Next, the cross-section was polished by sandpaper and a diamond-polishing compound. Then, the sample was etched by a 40% KOH solution in an ultrasonic bath at about 25^0C for 20 min to enhance the changes on the cross-section. SEM cross-sectional observations revealed that a structural change, which manifested itself as slight changes in contrast in the SEM photographs, occurred in the laser-irradiated section. Fig. 5.7 shows the SEM observation of the cross-section of the substrate after laser scanning with f = 500 kHz at v = 100 μm/s (left) and 800 μm/s (right). The changed regions appeared as aggregated cloud-like areas mixed with un-changed sections, with a comparatively paler gray contrast than the background. An inverted triangular shape was observed, in which the triangle was narrowest at the back surface, became wider toward the interior of Si, and disappeared at a certain position. The triangular shape of the changed region corresponds to the trace of the focused laser light.

I measured the Raman spectra of the modified region; however only the peak of the crystal Si was detected. Recently, Kammer et al. reported the transition from crystal Si to amorphous Si at a modified Si region using Raman microscope (Renishaw inVia Raman Microscope). Processing was performed using 800 fs laser pulses at a wavelength of 1,552 nm. The Raman peak of amorphous Si in the reported spectrum was approximately two orders of magnitude smaller than that of crystal Si [22]. In our Raman spectrum, in the modified areas of the sample cross-section, the Raman peak of the amorphous Si was difficult to discern. This might be attributed to the fact that the modified areas were mixed with the unchanged areas,

as shown in Fig. 5.7, rendering the Raman peak of amorphous Si too weak for detection by the Jasco Raman microscope.

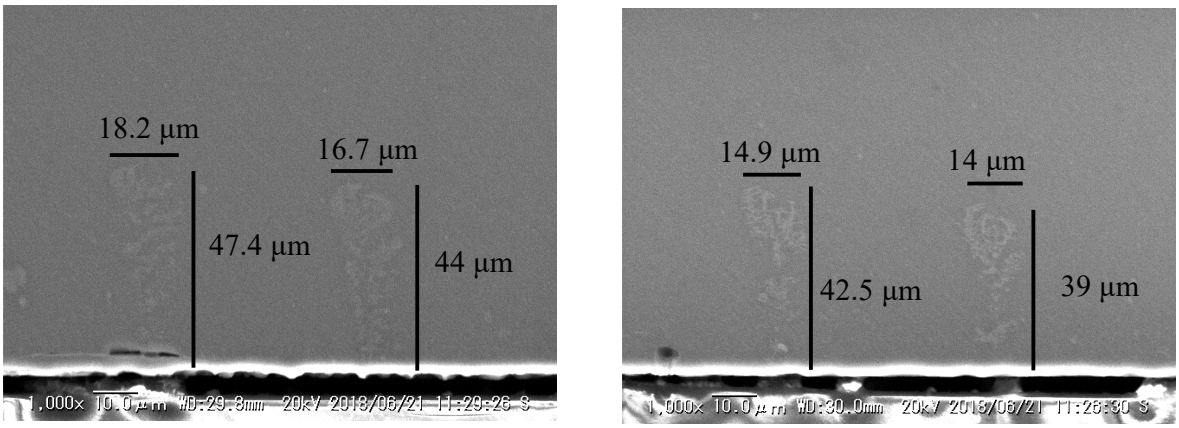

Scanning speed 100 μm/s

Scanning speed 800 μm/s

Fig. 5.7: SEM observation of the cross-section of the substrate after laser scanning with f = 500 kHz and v = 100 μm/s (left) and 800 μm/s (right). Changed regions appear as aggregated cloud-like sections mixed with unchanged areas and comparatively paler gray contrast than the background. An inverted triangular shape appeared, narrowest at the back surface and wider toward the interior of Si, eventually disappearing at a certain position. The triangular shape of the changed region corresponds to the trace of the focused laser light.

Although the micro-Raman observation of the changed areas showed only a crystalline silicon peak, some structural change should have occurred to cause the observed change in the contrast. The height of the modified region was defined as the distance from the back surface to the farthest position of the changed region, and the width of the changed region was defined as the maximum distance between two points at the same height. The widths of the change in the cross-section for v = 800 μm/s varied from 14 μm to 14.9 μm, which is smaller than the variation from 16.7 μm to 18.2 μm for v = 100 μm/s. These measured widths were nearly equivalent to the widths of the lines observed with IR light under microscopic observation, suggesting that the gray parts observed in the IR image should correspond to the structural changes inside Si. This implied that some energy was absorbed within the bulk Si.

5.5. Effect of scan speed *v*, repetition rate *f*, and focus position

I adjusted *v* determine whether the stability of the changes occurring on the Si back surface could be enhanced. With the same *f* = 500 kHz as in the previous experiments and *v* = 20 μm/s, which is 1/20th of the scan speed (*v* = 400 μm/s) used in the previous experiments, the changes within the Si (gray lines in IR images) were found to be continuous and stable; however the modifications on the back surface (dark lines in the visible images) appeared only as a fractions of the scanned lines. The percentage of changes on the back surface was defined as the ratio of the total length of the black lines to that of the gray lines, which was equivalent to the scan length. The changes on the Si back surface were more stable at a high *v* of 800 μm/s than at a lower *v*. The percentage change was approximately 80% in this case, whereas it was only approximately 20% for *v* = 100 μm/s. Pavlov et al. indicated that the optimum scanning speed for creating waveguides in the Si interior by a short pulse laser of 350 fs at 1.5 μm, pulse energy of 2 μJ, and a repetition rate of 250 kHz was in the range of 30–100 μm/s. They explained that the upper limit of the scanning speed was governed by the average heat deposited. In our case, with a 900 fs laser at nearly the same wavelength, such a limit could not be observed. Instead, the probability of machinability became lower with decreasing *v*, which corresponded to a higher amount of heat deposited at the irradiated positions. This showed that the amount of energy delivered to the back surface decreased owing to the increase in absorbed energy in the interior of Si. The percentage changes as a function of *v* are shown in Fig. 5.8. The average change (indicated by triangles) was calculated after measuring 10 processed lines under the same experimental conditions with the error bar representing the standard deviation. The figure also presents the width of the lines observed with IR light (indicated by circles), and that observed with visible light (indicated by squares) as functions

of *v*. Under the same experimental conditions, the width of the lines observed with IR light was larger than that observed with visible light. The percentage change occurring on the Si back surface decreased with decrease in *v*. In addition, the decrease in the width of the lines with lower *v* was noticed under both IR and visible observation.

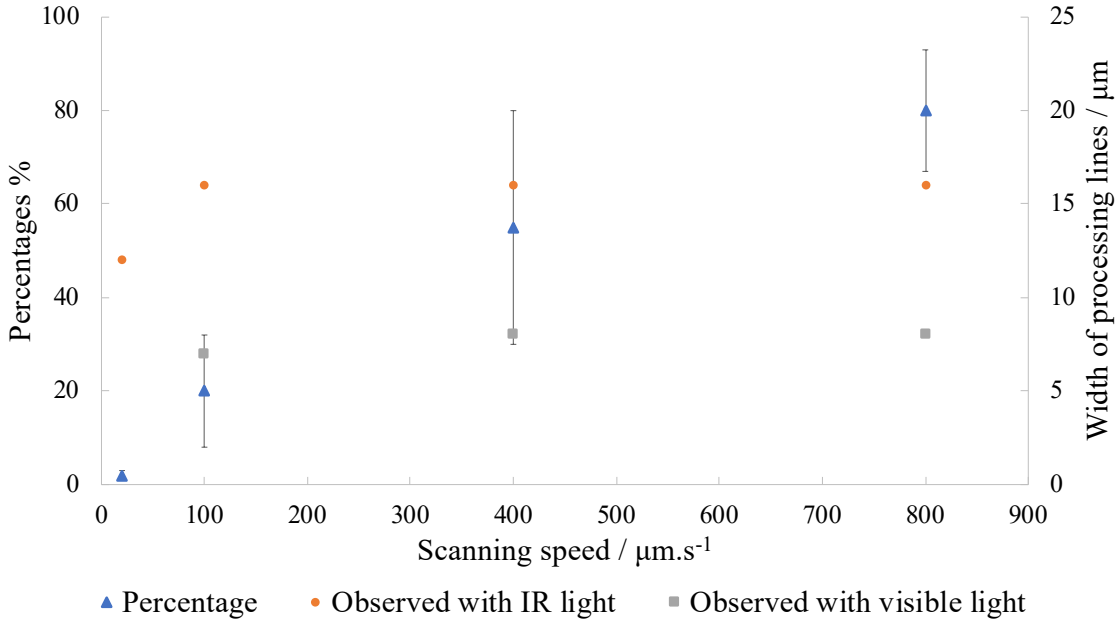

Fig. 5.8: Percentage change as a function of v. The average (indicated by triangles) was calculated after measuring 10 processing lines under the same experimental condition, with the error bar representing the standard deviation. The width of the lines observed with IR light (indicated by circles) and the width of lines observed with visible light (indicated by squares) are also shown.

Fig. 5.9 shows the effects of *f* on the processed lines. The observations of the back surface after scanning the sample at $v = 400$ µm/s and $f = 250$ kHz, 125 kHz, 50 kHz, and 10 kHz are shown sequentially from top to bottom in Fig. 5.9. With low *f* values of 10 kHz and 50 kHz, changes on the Si back surface occurred along the entire length of the processed lines. However, these changes occurred at only approximately 60% of the entire processed length for a higher *f* of 500 kHz. At low *f*, such as 10 kHz or 50 kHz, the changes were more stable, but

the lines observed with visible light were of white color, unlike the black color observed in the case of higher *f*. I used a laser microscope to obtain the depth profile along the processed lines. The largest depth values of the measurements at the 142 μm position at the center of each processed line was taken as the depth of the processed lines. For low *f*, the changes that occurred on the Si back surface had shallower depth of approximately 60 nm compared with the depth of 150 nm for *f* = 500 kHz. The decrease in depth was revealed as the change in color from black for higher *f* to white for lower *f* in visible micrographs. The widths of the lines observed with IR light were larger than those observed with visible light under all experimental conditions. The widths of the lines observed with visible light were nearly constant, approximately 8 μm for all *f*, whereas those observed with IR light decreased significantly for *f* less than 50 kHz.

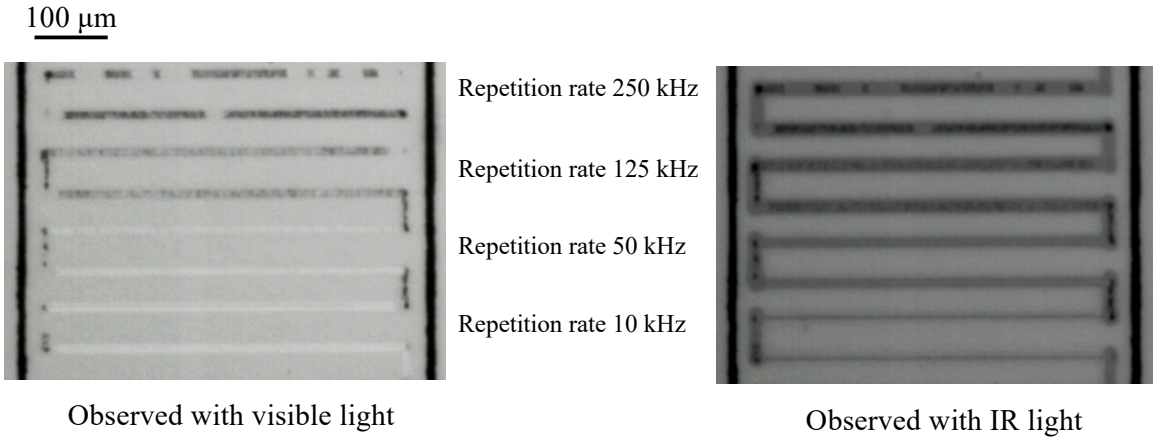

Fig. 5.9: Microscopy images observed with visible (left) and IR (right) wavelengths showing the effects of f on the processed lines. The scan speed was v = 400 μm/s.

As mentioned previously, parts of the laser-irradiated lines on the back surface contained a granular band or LIPSS morphology. At lower *f*, the structural changes on the back surface shifted to LIPSS with an interval of 270–330 nm, instead of the grain structures

observed at higher *f*. After laser scanning with f = 10 kHz at v = 400 μm/s, the entire processed area was covered by periodic structures being parallel to the laser polarization.

The impact of the focus position on the processing of the Si back surface was also investigated. The focus position was moved across the back surface, which was indicated as 0 on the back surface, "+" toward the interior of Si, and "−" toward the external positions from the surface of the substrate in μm. I scanned the laser with f = 500 kHz at v = 400 μm/s while adjusting the focus position from +3 to −9 μm in steps of 3 μm. No changes were apparent at the focus positions of +3 μm or −9 μm. The shifting of the focus position to below the Si back surface resulted in a decrease in the size of the changes observed on the Si cross-section. This demonstrated that more energy was absorbed in the interior of Si; thus, more energy reached the back surface. However, moving the focus position toward the interior of Si or far below the back surface increased the focal spot size on the back surface, resulting in decreased energy density on the back surface, which caused an inefficient machining rate at that.

5.6. Discussion

The modification observed on the Si back surface is revealed as a structural change of the Si crystals, possibly from crystalline to amorphous, which is manifested as a Raman peak on the back surface. Nevertheless, the presence of the amorphous Si phase in the modified part within the substrate was not detected. This might be due to the inadequate sensitivity and intensity of the Raman signal for analysis of the structural change in the Si interior. The material properties of amorphous Si are significantly different from those of crystalline Si. For example, the band gap increases from 1.1 eV in crystalline Si to 1.6 eV in amorphous Si [44] and the absorption coefficient of amorphous Si is higher than that of crystalline Si. The refractive indices also change; thus, absorption or refraction at the boundary of the amorphous

Si is shown as a gray contrast in the IR micrographs. To induce such a change, certain portions of the laser energy should be absorbed within the substrate, even though the laser is not strongly focused at the position where these changes are observed. Judging from the focus conditions required to induce the machining on the Si front surface by the laser, this absorption is not due to the non-linear processes, as the laser power density of a single pulse is considered to be too low for such processes. Therefore, this absorption should be attributed to the effects of multiple pulse irradiation. Under our experimental conditions, a large number of laser pulses are irradiated at the same spot, resulting in a high accumulation of energy at one spot. This will lead to a local increase of temperature at the spot, which increases the absorption coefficients of the laser light caused by both the linear and nonlinear processes, owing to a higher density of thermally excited electrons. The absorption coefficient of Si significantly increases with temperature [45]. Because of the heat diffusion along the incoming laser axis, the absorption point moves upstream of the laser beam as the number of irradiated pulses increases. The area of the absorption region increases when the absorption point extends upstream of the laser path in the substrate, resulting in the reduction of the energy density. Hence, the modification stops at a certain point in the interior of Si, where it leaves a triangular region of change. Similar movement of the absorption point was reported by Miyamoto et al. in glass welding by a high-repetition-rate ultra-short laser [46]. This induces non-local absorption of the laser energy along the laser path. Consequently, the percentage of energy reaching the Si back surface decreases; thus, significant ablation is prevented from occurring on the back surface.

Fig. 5.10 shows the dependences of the cross-sectional changes and the width of the gray lines in IR microscopic observation from the back surface on laser scanning speed v with f = 500 kHz. The average was calculated after measuring six processed regions under identical

experimental conditions. The height of the cross-sectional change (indicated by triangles) increases with decrease in *v*. I also examined the dependence of the cross-sectional changes on *f* at *v* = 400 μm/s. With decrease in *f* from 500 kHz to 125 kHz, the width and height of the cross-sectional change increases from 14 μm and 43 μm to approximately 17 μm and 63 μm, respectively. Nevertheless, when *f* is smaller than 125 kHz, the size of the change is reduced significantly. Under the similar experimental conditions, the width of the cross-sectional changes (indicated by diamonds) was nearly equal to the width of the gray lines observed on the Si back surface with IR light (indicated by circles).

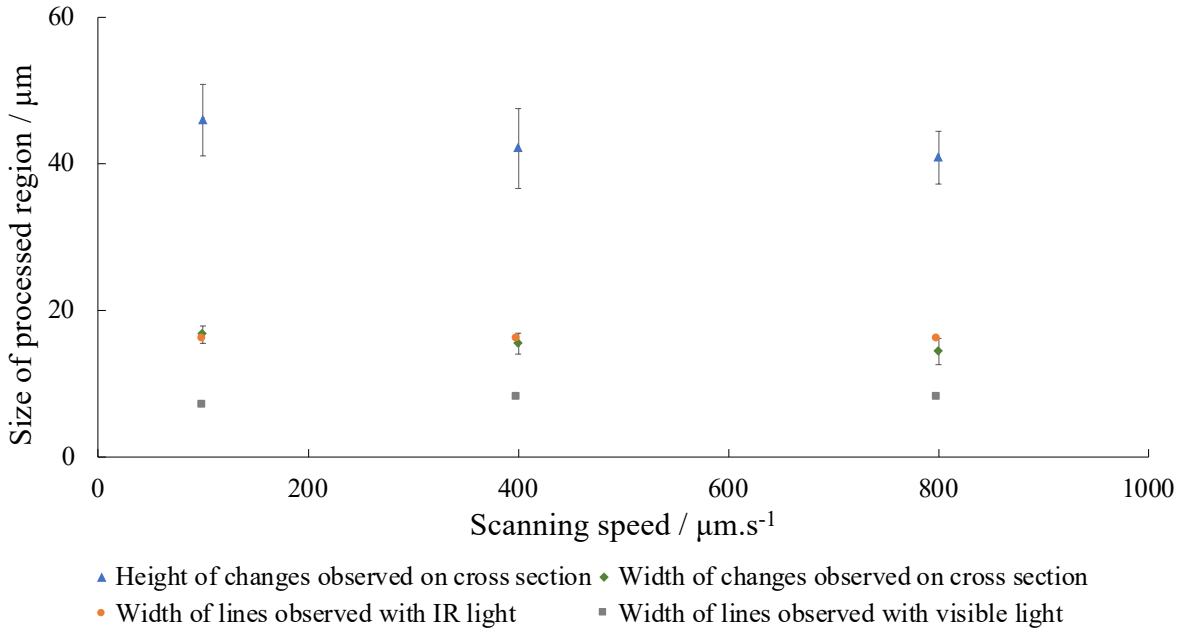

Fig. 5.10: Dependence of the cross-sectional changes and the width of gray lines on the Si back surface in microscopic observation from the back surface on laser scanning speed v with f = 500 kHz. The average was calculated after measuring six processing regions under the same experimental conditions.

With higher *v* or lower *f*, the number of laser pulses irradiated at one position decreases and the interval between successive pulses increases, which decreases the amount of heat accumulated at the position. Thus, the heat effects at the laser path becomes smaller and the energy loss caused by the internal change becomes less, allowing a larger amount of laser

energy to reach the back surface and stabilizing the changes on the back surface. However, the number of pulses irradiated at the same spot decreases, and the extent of the ablation becomes smaller owing to the smaller amount of energy. This explains the stability of the changes occurring on the back surface as well as the shallower depth of the groove for lower *f*.

Even under similar experimental conditions, the size of the changes observed on the Si cross-section was not constant. This instability may be explained by the residual stresses induced by the preceding pulses [47]. The main reason for the development of stress in the bulk Si would be the volume change of the newly formed amorphous Si. The slight variations in the local properties, such as the residual stress due to the polishing process of the substrates, and the concentration of dopants, impurities, and/or defects, cause slight changes in the initial stage of the absorption process, which is amplified in the subsequent absorption steps of the multiple pulses with increase in the local temperature. Furthermore, the absorption increases, and the process continues until the heat accumulated at the position is in balance with the heat diffused into the surrounding substrate. This causes a variation in the absorbed laser energy in the substrate as well as in the energy delivered to the back surface, resulting in unstable processed lines on the Si back surface. This finding is in accordance with the conclusion of Grojo et al. that the energy deposition of the femtosecond laser pulses results in non-uniform material changes [48]. To machine the back surface of Si, the power density of the laser pulse is suggested to be low to avoid nonlinear absorption along its path, whereas the total laser energy should be sufficiently high to induce ablation on the back surface.

VI. Wet Etching of Silicon Back Surfaces Using 1,552.5 nm Femtosecond Laser

6.1. Background information and purpose

Even though several techniques are available for the fabrication of silicon-based devices, efficient three-dimensional (3D) microfabrication techniques in particular are in high demand, especially for producing micrometer-scale 3D structures [49-51]. I have demonstrated that micromachining through an Si substrate by a femtosecond laser at 1,552.5 nm is possible. However, only shallow grooves were formed so far; its depth was approximately 170 nm or less.

Therefore, to increase the machining rate, I tried laser-assisted wet-etching using KOH solution. The laser irradiation process can modify the rate of etching of Si by an etchant. Thus, by combining laser irradiation and treatment with an etchant, one can produce 3D structures on Si substrates. However, this process is a multistep one and usually takes a lot of time [52]. Further, while the etch rate of Si during laser-assisted wet etching is higher than that during etching in the absence of a laser, there are a few problems with the practical applicability of this method. For instance, the laser is usually irradiated onto the substrate through a liquid layer. This inevitably results in thermally induced bubbles near the position of irradiation. These phenomena can block or distort the incoming laser beam, resulting in unsteady and uncontrollable processing [53]. In addition, laser irradiation on a liquid layer perturbs the free liquid surface, resulting in the uncontrollable reflection/refraction of the incoming laser beam [54]. Furthermore, the debris produced tends to get deposited or suspended near the position or within the machined structure.

By performing wet etching on the back surfaces of the Si substrates, one can avoid these problems. Niino's group proposed laser-induced backside wet etching for the 3D machining of transparent substrates. In this process, a pulsed laser is irradiated onto the substrate and is absorbed by the liquid that is in contact with the back surface of the substrate; this produces a laser-induced plasma, which machines the substrate [55, 56]. In addition, it is a debris-free process. The 3D laser processing of transparent dielectric materials by short-pulse lasers via nonlinear absorption processes is also an established method for fabricating 3D structures on or within these materials [57-59].

The back surfaces of the Si substrates were maintained in contact with an etchant liquid. Thus, it was possible to avoid the problems encountered during conventional laser-assisted wet etching. Liu et. al. reported the processing of the back surfaces of Si wafers with nanosecond Nd:YAG laser pulses in air [60]. They reported the melting and transition of crystalline Si into oxidized and amorphous Si by heating via linear absorption of the laser radiation, because Si weakly absorbed the laser radiation of 1064 nm. Here, I report the results of further attempts on wet etching of the back surfaces of Si substrates by irradiation with the pulses of a femtosecond 1,552.5 nm laser through the substrates. The absorption of the laser radiation by Si is considered to be a non-linear process and thus more localized processing would occur. While the preliminary results have been reported elsewhere, I encountered difficulties during the experiments, which included a low machining rate and unsteady processing [25, 61]. The maximum groove depth did not always follow the expectation since at some focus position, deeper groove was formed while scanning by lower laser density or higher scanning speed. It can be thought that the hydrogen bubbles caused from the chemical reaction between Si and KOH block the contact of Si and KOH. In etching, hydroxide ions and water act as a reactant

together; Si reacts with water and hydroxide ions, then generate the hydrogen gas. Regardless of the etching solution, chemical formula of the alkali etching is as follows:

$$Si + 2H_2O + 2OH^- \rightarrow Si(OH)_2(O^-)_2 + 2H_2\uparrow$$

In case of using KOH as etchant:

$$Si + H_2O + 2KOH \rightarrow K_2SiO_3 + 2H_2\uparrow$$

These bubbles formed, moved, disappeared and deformed again continuously during the laser scanning. It leads to the situation at which the groove depth varied significantly even though the focus position shifted only 1 μm. The number of bubbles tends to grow more quickly with the increase of laser power but their lifetime and size has not been investigated.

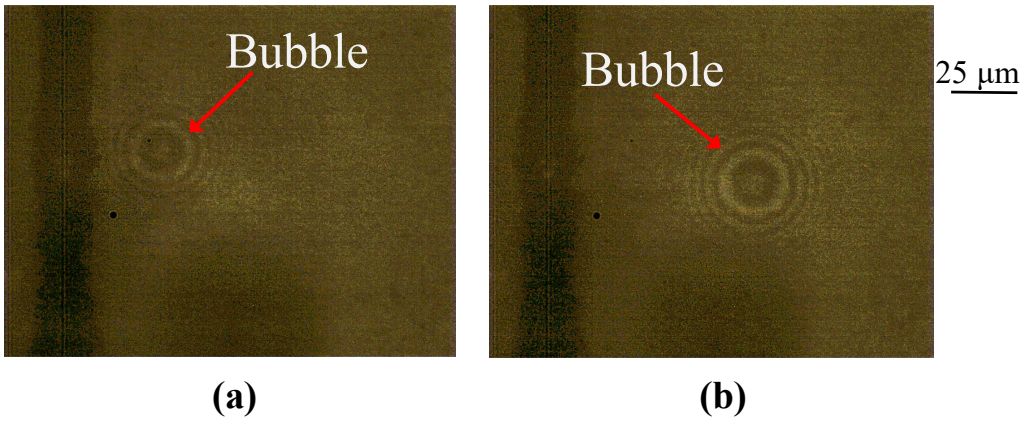

Fig. 6.1: Bubble formation during the experiment (a) at one moment and (b) after 2 seconds.

6.2. Experimental

Given that the etch rate at the Si back surface would be higher, wet etching using an aqueous KOH solution was performed. During the wet etching process, a 40% KOH solution at 25°C was maintained in contact with the Si back surface, while the laser was irradiated on its front surface.

During trial experiments, I observed that bubbles formed during the irradiation process and that they prevented stable contact between the Si substrate surface and the KOH solution, resulting in nonuniform grooves along the processing. Therefore, I designed an irradiation cell, which is shown in Fig. 6.2. The Si substrate (20 mm x 20 mm) was placed on the top of the liquid cell, in which the 40% KOH solution was circulated continuously using a pump. The back surface of the substrate was in complete contact with the etchant liquid such that the flowing liquid carried away the bubbles formed at the irradiated position.

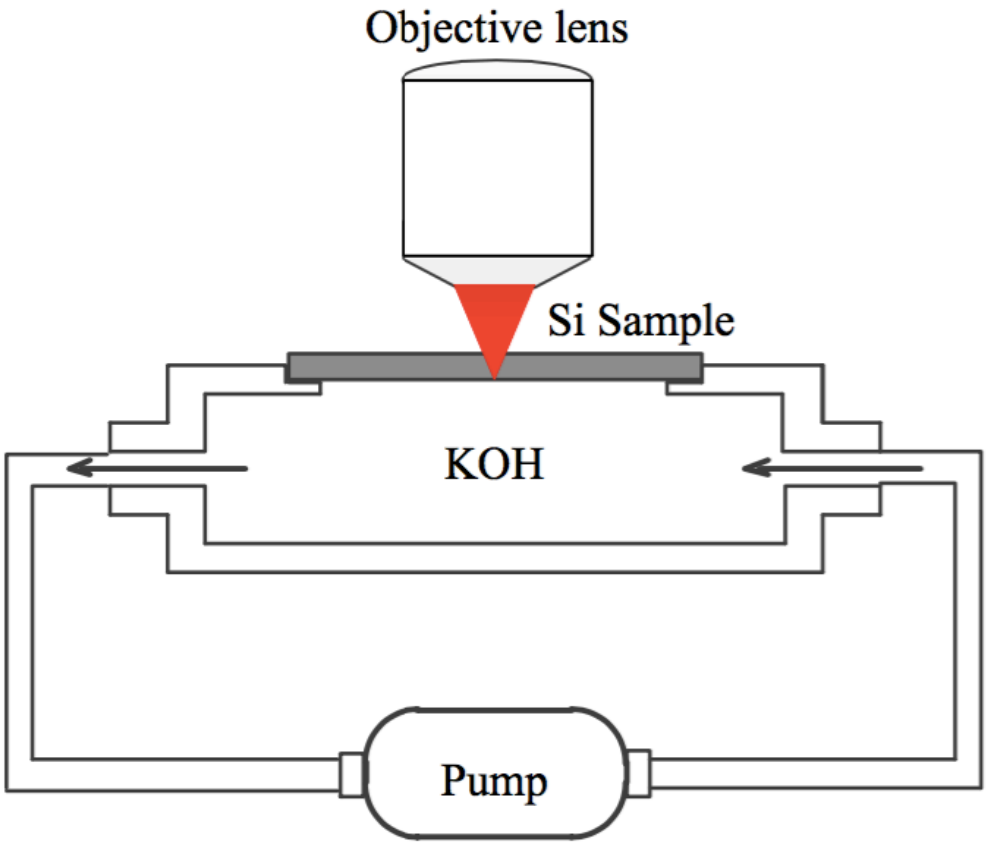

Fig. 6.2: Schematic of irradiation cell with flow system

6.3. Results

Figure 6.3 shows optical micrographs of the Si back surfaces obtained at visible-range and IR wavelengths after wet etching during irradiation at f = 500 kHz; v = 50 μm/s and the focus position was at -15 μm. I would like to emphasize here that there was no observable change on the front surface of the Si substrate, where the irradiated laser was incident. The laser scans appeared as black in the visible-light and IR images were the grooves etched on the back surface. In the visible-light images, only the changes that occurred on the back surface could be observed. Thick black parts corresponded to deep grooves as shown in Fig. 6.3 while thinner straight lines were shallow grooves. Also, I did not observe any debris sticking around the processed lines as expected for a backside wet etching. This indicated that this method was a debris-free one. On the other hand, in the IR images, at some parts, slightly thicker gray lines appeared along the scan lines with thinner black parts. As reported in chapter V, the gray parts observed with IR light are the changes occurring only inside Si. The IR images showed the changes that had occurred both on the back surface and within the substrate, in keeping with a previous report. Even though a flow system had been used to avoid a bubble formation, the groove depth showed variations, ranging from a few hundred nanometers to a few micrometers. The etch rate was significantly higher compared to that during dry etching. In case of wet etching, at some positions, the maximum etch depth was nearly 8 μm, compared to the maximum of 150 nm in case of dry etching. However, as stated above, the etch depth along the processing path showed significant variations.

It was expected that the KOH solution would have an effect on the Si substrate even in the absence of laser irradiation. In the irradiation system used in this study, the Si back surface was in contact with the solution for some time prior to the laser irradiation process, and this

contact period increased from the start position of the laser scan to its end. I defined the pre-etch time as the period in which the Si back surface and the KOH solution were in contact before the start of the laser irradiation process. In our experiments, the pre-etch time was 60 s, after which the irradiation process was started. Further, the pre-etch time increased from the top to the bottom for the scans performed in this order.

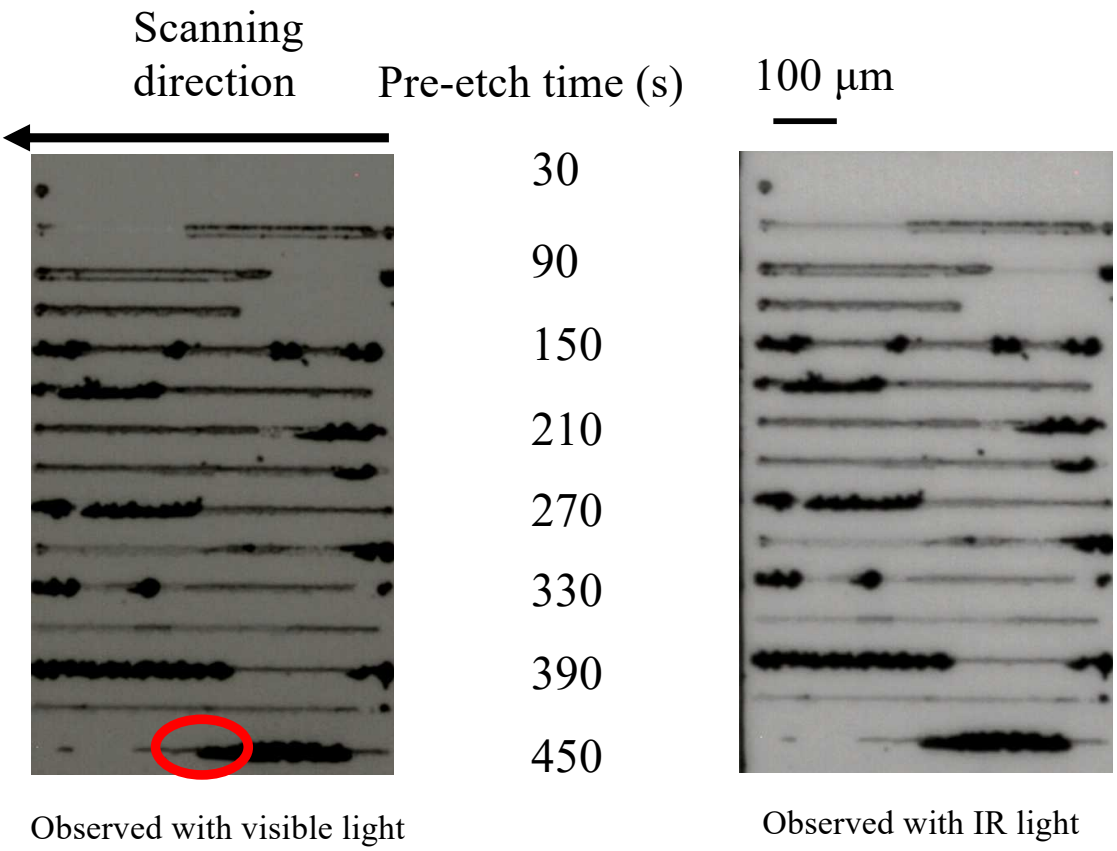

Fig. 6.3: Visible-light (left) and IR (right) microscopy images of Si back surface after wet etching at f = 500 kHz and v = 50 µm/s at -15 µm focus position

I measured the etch depth of the black area marked with the circle in Fig. 3 using a laser microscope; the pre-etch time in this case was 450 s. Figure 6.4 shows the depth profile along a length of 142 µm at the center of the black area. I considered the distance between the lowest part to the surface of the Si substrate to be the etch depth. The maximum groove depth was

approximately 7.76 μm. The depth varied significantly along the processing path, even though no bubble was observed on the back surface during irradiation either with a naked eye or using the IR camera. Moreover, even when the focus position, *f*, and *v* were changed, similar variations were observed. The same variations in etch depth were observed for dry etching case but the absolute depth was much shallower than wet etching case.

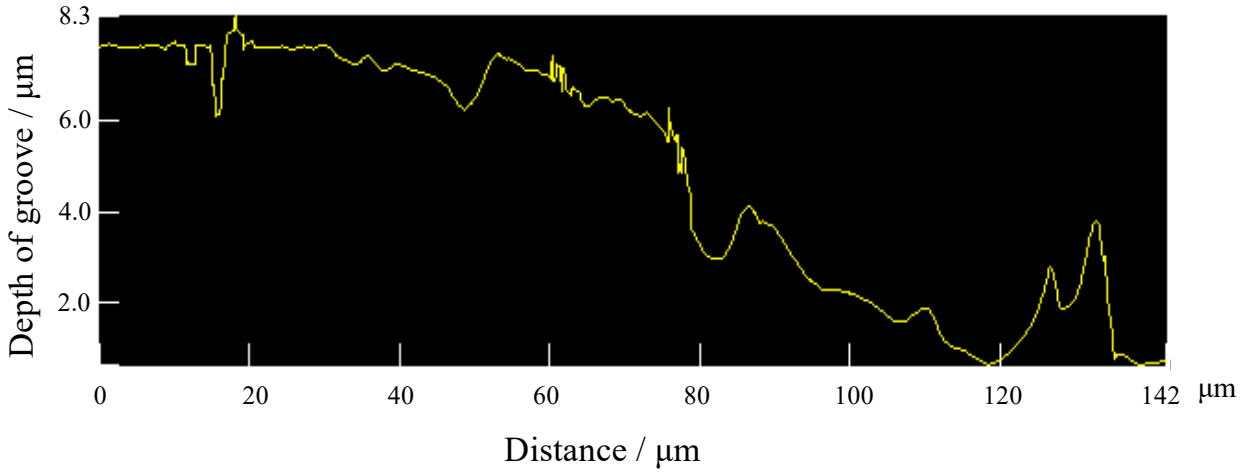

Fig. 6.4: Depth profile of 142-μm-long section at center part of processing line for pre-etch time of 450 s. Position corresponds to circle in Fig. 6.3.

6.4. Effect of focus position

Figure 6.5 shows visible-light and IR images of a back surface subjected to wet etching at the same *f* and *v*; however, in this case, the laser was irradiated at the 0 μm focus position. The lines in the visible-light image are narrower and fainter compared to those shown in Fig. 6.3. In addition, the lines were not continuous but intermittent, and there was no thick part, indicating that the etch depth was less than that in the case for a focus position of -15 μm. In the IR image, the black dotted lines, which correspond to those observed in the visible-light image, overlap with wider, continuous gray bands. These gray bands represented the changes

that occurred within the Si substrate and were not observed in the images in Fig. 6.3, which corresponded to a focus position of -15 μm. The depth of the grooves formed at a focus position of 0 μm was approximately 300 nm and shallower than that of the grooves formed at -15 μm but greater than that of grooves formed by the dry etching of the back surface (approximately 150 nm). Thus, the focus position of -15 μm resulted in a higher etch rate (deeper grooves) compared to the 0 μm position. I tried other focus positions as well, namely, -12, -9, -6, -3, and +3 μm. For long enough pre-etch time (360 s and longer), at the -12 μm focus position, I could achieve an etch depth of 8 μm at some points along the processing path. However, when the focus position was moved closer to the Si back surface, the maximum depth decreased. When I set the focus position to be within the Si substrate (+3 μm), the maximum etch depth on the Si back surface was very low, approximately 300 nm. Thus, it can be concluded that the laser must be focused at a point that lies beneath the etchant surface in order to increase the etch rate.

By performing laser-assisted wet etching on the back surfaces of Si substrates, I could form grooves with greater depths than that formed by dry etching. However, the depth of the grooves was not constant. For the same v and f values and focus position, the depth along the same processing path varied significantly from point to point. Even though the changes induced on the Si back surfaces were more uniform after the wet etching process than dry etching, I could not etch uniform and continuous deep grooves.

The etch rate at the -15 μm focus position was greater than that at the 0 μm position, even though the power density at the back surface was much lower in the former case. This contradictory result can be explained as follows. The optical absorption coefficient of water at 1,552.5 nm is approximately 9.5 cm^{-1} [62], and that of KOH solution is considered to be similar

to that of water. Thus, owing to the high absorption coefficient of water, the aqueous KOH solution absorbed energy from the laser via a linear absorption process. Given the refraction of the laser light at the silicon-liquid interface, the focus position at -15 μm actually corresponded to a position 6.12 μm within the solution below the Si back surface under tight focusing. Thus, a small focal volume of the liquid close to the Si back surface absorbed a large amount of the laser energy, resulting in a rapid increase in its temperature. As a result, the etch rate of Si was high. At the 0 μm focus position, similar to dry etching, wherein nonlinear absorption occurred within the Si substrate near the focus. This decreased the amount of laser energy that reached the focus position. Hence, the temperature of the KOH solution in contact with the surface was lower than that at -15 μm, resulting in shallower depth.

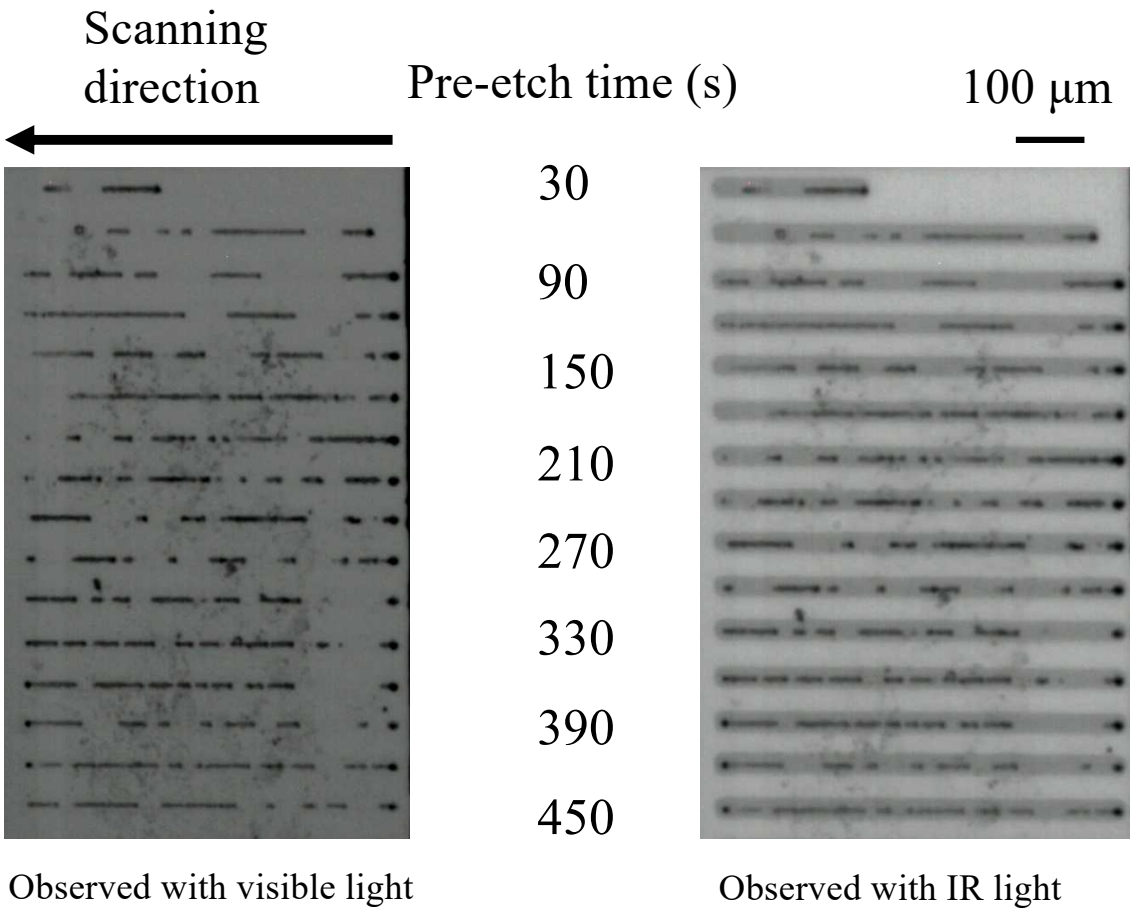

Fig. 6.5: Optical microscopy images of Si back surface obtained using visible (left) and IR (right) light after wet etching at f = 500 kHz and v = 50 μm/s at 0 μm focus position.

6.5. Effect of scan speed *v* and laser repetition rate *f*

Figure 6.6 shows microscopy images of the back surface of a Si substrate after it has been subjected to wet etching at the 0 μm focus position at f = 500 kHz and different v values: 4 lines at 800 μm/s, 4 lines at 400 μm/s, 4 lines at 100 μm/s, and 2 lines at 20 μm/s. Although the pre-etch time inevitably increased from the top lines to the bottom ones, as those shown to Figs. 6.3 and 6.5, its effect was not evident in these images. I could form continuous grooves, with the contrast of the lines becoming sharper with a decrease in v. At the lowest v value (20 μm/s), dotted lines were observed, suggesting that etching had occurred in a discontinuous manner. The average groove depth was approximately 400 nm and greater than that for v = 800 μm/s, which was approximately 200 nm. Continuous gray lines were seen in the IR images in addition to the black lines at the center, which corresponded to those observed in the visible-light images. The widths of the gray lines were greater than those of the lines observed in the visible-light images, indicating that the internal changes induced within the substrate had occurred over a wider area than those on the back surface.

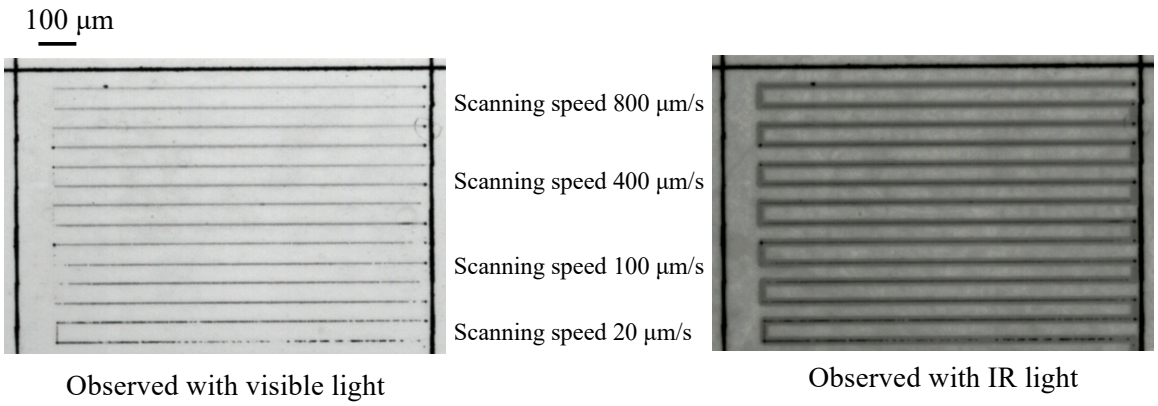

Fig. 6.6: Visible-light (left) and IR (right) images of Si back surface after wet etching at f = 500 kHz and different v at 0 μm focus position. From top to bottom: 4 lines at 800 μm/s, 4 lines at 400 μm/s, 4 lines at 100 μm/s, and 2 lines at 20 μm/s. Black rectangular lines are marking made by direct laser irradiation for adjusting focus.

I performed laser scans at v = 50 μm/s at the 0 μm focus position with different f: 250 kHz, 125 kHz and 50 kHz (Fig. 6.7). Even at the lowest f value of 50 kHz, continuous etch lines were formed. Moreover, the average depth did not change significantly with different f and remained at approximately 250-300 nm along each processed line. The internal changes observed in the IR images were continuous; however, in this case, the width decreased slightly with the decrease in f. Since the number of pulses irradiated at the same spot decreased with the decrease in f, the total amount of energy transmitted also decreased, resulting in a smaller internal modified area.

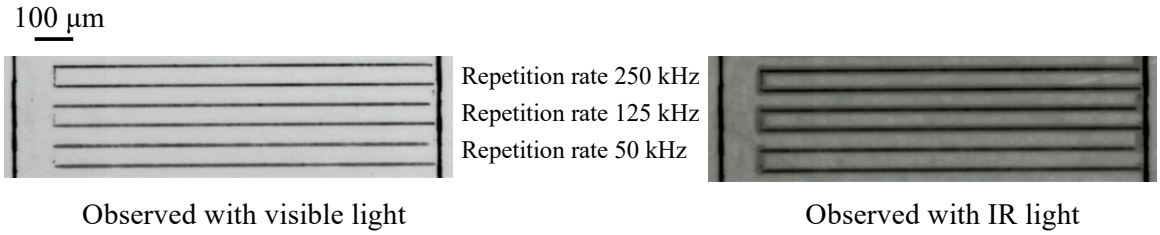

Fig. 6.7: Visible-light (left) and IR (right) images of Si back surface after wet etching at v = 50 μm/s and different f at 0 μm focus position. From top to bottom: 2 lines with 250kHz, 2 lines with 125kHz, and 2 lines with 50kHz. Black rectangular lines are marking made by direct laser irradiation for adjusting focus.

6.6. Morphology on back surface after wet etching

During SEM observations, two types of morphologies were observed after the laser-assisted wet etching at v = 400 μm/s at the 0 μm focus position, namely, grooves and periodic structures oriented perpendicular to the laser polarization direction. At the 0 μm focus position, for f = 250 kHz and lower, periodic structures were formed, while at f = 500 kHz, both grooves and periodic structures were formed. I estimated the periodicity of these structures by measuring the distance between six consecutive parallel lines and dividing it by 5. The interval was found to be approximately 200 nm, and the depth was approximately 170-300 nm. These values were different from those of the periodic structures formed during dry etching; in this case, the interval was approximately 330 nm, and the structures were oriented parallel to the laser polarization direction. However, when the laser was focused at a position deeper within the KOH solution, other types of structures were formed. Figure 6.8 shows SEM images of a processing line after wet etching at f = 500 kHz and v = 50 μm/s at the focus positions of (a) 0 μm and (b) -15 μm. At the 0 μm focus position, the back surface was dominated by periodic structures oriented perpendicular to the laser polarization direction. Meanwhile, at the -15 μm focus position, in some parts of the processing line, I observed periodic structures oriented parallel to the laser polarization direction and having an interval of approximately 1.2 μm and depth of 1.3 μm. Note that magnifications in (a) and (b) are different. Some parts of the line were deep grooves with a depth of up to 5 μm, with no periodic structures being present. Figure 6.8 (c) shows an SEM image of a processing line after wet etching at f = 500 kHz and v = 100 μm/s at the -15 μm focus position. Figure 6.8 (d) showed the center of Fig. 6.8 (c), at which periodic structures oriented perpendicular to the laser polarization direction and having an interval of approximately 200 nm were observed; these were similar to the structures observed

at the 0 μm focus position shown in (a). The depth of these periodic structures was low at approximately 200-300 nm. However, at the edge of the processing line, periodic structures parallel to the laser polarization direction were observed. Their interval was approximately 1.2-1.3 μm, and the depth was 0.8-1.5 μm.

After the wet etching process, I found so-called laser-induced periodic surface structures (LIPSS) or ripples at the bottom of the etched grooves. I believe this is the first instance where LIPSS were formed on the back surface of an Si substrate in an aqueous solution. There have only been a few studies on the formation of LIPSS at under water conditions [62, 63], and in these previous studies, the LIPSS were formed on the front surface of the Si substrate under direct irradiation. Hence, the formation of LIPSS on the back surfaces of Si substrates in water is a unique achievement. The formation of LIPSS on materials surfaces is a subject of significant research interest, and a more detailed description of the LIPSS formation on the Si back surfaces can be found elsewhere.

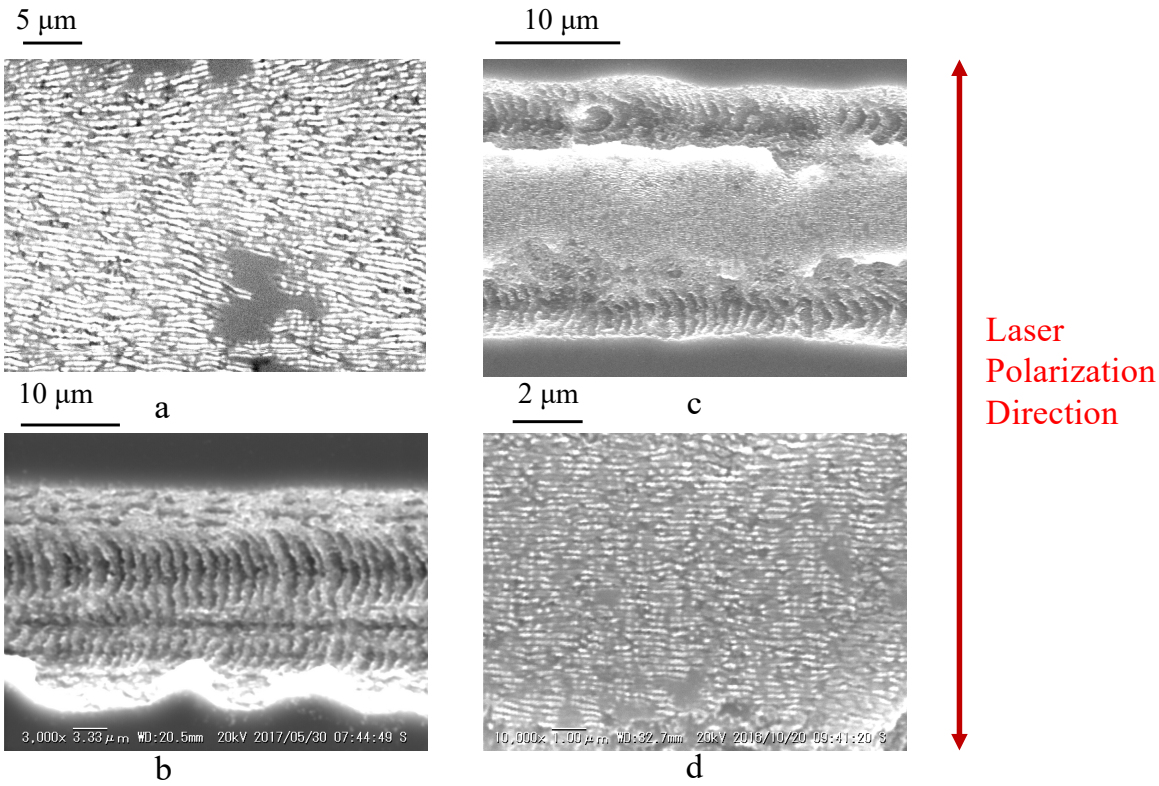

Fig. 6.8: SEM images of LIPSS formed on Si back surface after wet etching at f = 500 kHz and v = 50 µm/s at (a) 0 µm and (b) -15 µm focus positions and (c) at v = 100 µm/s at -15 µm focus position. (d) shows the center region of figure (c).

VII. Conclusion

I presented my attempt to machine 3D microstructures on Si using a femtosecond laser of 1,552.5 nm wavelength. Although I demonstrated that the interior and back surface of the Si substrates could be modified without any noticeable change on the front surface, these changes occurred unstably, especially on the back surface. An incubation effect was observed in the modification of the interior and back surface of the Si substrate. The changes that occurred inside the Si substrate were revealed as continuous lines of gray contrast in the IR micrographs. However, the changes on the back surface appeared as black images in the visible/IR micrographs and were not continuous but intermittent under most irradiation conditions. SEM observations indicated that the modifications on the back surface appeared as granular structures or LIPSS with only shallow groove formation, if any. The impacts of the repetition rate f and the scan speed v of the laser were studied and the results suggested that heat accumulation due to multiple pulse irradiation causes an increase in the local temperature and absorption along the incident laser path, which prevents the delivery of sufficient energy to induce ablation on the back surface. Additionally, deep grooves cannot be obtained under conditions for stable processing on the back surface. It is believed that using lasers with higher pulse energy and shorter pulse width at longer wavelengths than what was used in this study can enable the selective machining of 3D structures on the back side and the interior of Si substrates, which I intend on exploring in a future study.

I also tried to improve the etch rate by performing the laser-assisted wet etching of Si back surfaces using a femtosecond laser at 1552.5 nm. The etch rate on the back surface during the wet etching process was higher than dry etching, resulting in an increase in the groove depth from 300 nm to approximately 6 μm. I also examined the effects of laser repetition rate,

the scanning speed and focus position on the wet etching process. A focus position approximately 12-15 μm below the Si back surface and within the KOH solution was found to be the most appropriate one for ensuring that the depth of the etched lines was the maximum. However, at the -15 μm focus position, which resulted in deeper grooves, the groove depth showed significant variations. At the 0 μm focus position, the depth was shallower than -15 μm focus position but was deeper with better uniformity than that during dry etching. The morphology of the structural changes induced on the Si back surface by the laser-assisted wet etching method was different from that of the structures machined by the dry etching method. In the former case, grooves and periodic structures either parallel or perpendicular to the laser polarization direction and having different depths were observed. The underlying formation mechanism of these structures will be elucidated in a future study.

In conclusion, this research suggests that it is possible to modify the interior or backside of Si by infrared femtosecond laser. Higher peak power may enable more stable and selective machining of Si. As a result, I can expect to find out the more accurate relationship between laser conditions or scanning speed with the structural changes on Si back surface in both cases; dry etching and wet etching. Both the refractive index changes on Si and structural changes on Si surface has many promising values on Si application in real worlds.

List of references

1. A. Golshan, B. T. H. T. Baharudin, H. Aoyama, M. K. A. M. Ariffin, M. I. S. Ismail, and A. A. Ehsan, “Ultraprecision machining of silicon wafer by micromilling process,” Proc. Eng. 184, 192–196 (2017).

2. J. Steffens, M. A. Fazio, D. Cavalcoli, and B. Terheiden, “Multi-characterization study of interface passivation quality of amorphous sub-stoichiometric silicon oxide and silicon oxynitride layers for photovoltaic applications,” Sol. Energy Mater. Sol. Cells 187, 104–112 (2018).

3. H. Yilong, “Silicon-based MEMS fabrication techniques and standardization,” Indian J. Pure Appl. Phys. 45, 317–320 (2007)

4. J. Bonse, S. Baudach, J. Kruger, W. Kautek, and M. Lenzner, “Femtosecond laser ablation of silicon-modification thresholds and morphology,” Appl. Phys. A 74, 19–25 (2002).

5. Y. Ito, H. Sakashita, R. Suzuki, M. Uewada, K. P. Luong, and R. Tanabe, “Modification and machining on back surface of a silicon substrate by femtosecond laser pulses at 1552 nm,” J. Laser Micro/Nano Eng. 9, 98 (2014).

6. A. Yadav, H. Kbashi, S. Kolpakov, N. Gordon, K. M. Zhou, "Stealth dicing of sapphire wafers with near infrared femtosecond pulses" Appl Phys A 123, 369 (2017).

7. A. Couairon, and A. Mysyrowicz. "Femtosecond filamentation in transparent media", Phys Rep 441, 47–189 (2007).

8. P. Simon and J. Ihlermann, “Machining of submicron structures on metals and semiconductors by ultrashort UV-laser pulses,” Appl. Phys. A 63, 505–508 (1996).

9. X. Jia and X. Zhao, “Numerical study of material decomposition in ultrafast laser interaction with metals,” Appl. Surf. Sci. 463, 781–790 (2019).

10. A. H. Hamad, "Effects of Different Laser Pulse Regimes (Nanosecond, Picosecond and Femtosecond) on the Ablation of Materials for Production of Nanoparticles in Liquid Solution", High Energy and Short Pulse Lasers (2016).

11. C. Y. Chien, " Pulse Width Effect in Ultrafast Laser Processing of Material", Applied Physics A 81(6):1257-1263 (2005).

12. Y. Shimotsuma, K. Hirao, P. G. Kazansky, and J. Qiu, “Three-dimensional micro- and nano-fabrication in transparent materials by femtosecond laser,” Jpn. J. Appl. Phys. 44, 4735 (2005).

13. W. Watanabe, Y. Li, and K. Itoh, “Ultrafast laser micro-processing of transparent material,” Opt. Laser Technol. 78, 52–61 (2016).

14. A. H. Nejadmalayeri, P. R. Herman, J. Burghoff, M. Will, S. Nolte, and A. Tünnermann, “Inscription of optical waveguides in crystalline silicon by mid-infrared femtosecond laser pulses,” Opt. Lett. 30, 964 (2005).

15. Y. C. Lam, D. V. Tran, H. Y. Zheng, V. M. Murukeshan, J. C. Chai, and D. E. Hardt, “Surface damage of crystalline silicon by low fluence femtosecond laser pulses,” Surf. Rev. Lett. 11, 217–221 (2004).

16. A. Stone, M. Sakakura, Y. Shimotsuma, K. Miura, and K. Hirao, "Femtosecond Laser-Writing of 3D Crystal Architecture in Glass: Growth Dynamics and Morphological Control", Mater Des 146, 228–238 (2018).

17. K. Zoschke, T. Fischer, M. Toepper and K. D. Lang, "Polymide based temporary wafer bonding technology for high temperature compliant TSV backside processing and thin device handling", Proceedings of Electronic Components and Technology Conference (2012).

18. D. V. Tran, Y. C. Lam, H. Y. Zheng, V. M. Murukeshan, J. C. Chai, and D. E. Hardt, “Femtosecond laser processing of crystalline silicon”, Innovation in Manufacturing Systems and Technology (2005).

19. S. Leyder, D. Grojo, P. Delaporte, W. Marine, M. Sentis, and O. Utéza, “Multiphoton absorption of 1.3 μm wavelength femtosecond laser pulses focused inside Si and SiO_2,” Proc. SPIE 8770, 877004 (2013).

20. V. V. Kononenko, V. V. Konov, and E. M. Dianov, “Delocalization of femtosecond radiation in silicon,” Opt. Lett. 37, 3369–3371 (2012).

21. P. C. Verburg, G. R. B. E. Römer, and A. J. Huis in ‘t Veld, “Two-photon–induced internal modification of silicon by erbium-doped fiber laser,” Opt. Express 22, 21958–21971 (2014).

22. I. Pavlov, O. Tokel, S. Pavlova, V. Kadan, G. Makey, A. Turnali, Ö Yavuz, and FÖ Ilday, “Femtosecond laser written waveguides deep inside silicon,” Opt. Lett. 42, 3028–3031 (2017).

23. H. Kammer, G. Matthaus, S. Nolte, M. Chanal, O. Uteza, and D. Grojo, “In-volume structuring of silicon using picosecond laser pulses,” Appl. Phys. A 124, 302 (2018).

24. H. Kammer, G. Matthaus, K. A. Lammers, C. Vetter, M. Chambonneau, and S. Nolte, “Origin of waveguiding in ultrashort pulse structured silicon,” Laser Photonics Rev. 13, 1800268 (2019).

25. Y. Ito, R. Tanabe, and K. Tada, “Nonlinear micro-processing of silicon by ultrafast fiber laser at 1552 nm,” MRS Proc. 1365, 2–5 (2011).

26. Y. Ito, Y. Morita, H. Sakashita, R. Suzuki, R. Tanabe, H. Sakurai, K. Tada, "Micromachining through Silicon Substrates by Ultrafast Laser at 1552 nm", Applications of Lasers and Electro-Optics, Vol.105, 1102-1107 (2012).

27. R. Suzuki, N. Tsujisaka, R. Tanabe, and Y. Ito, “Laser induced forward transfer of gold film on silicon substrate using an infrared femtosecond laser,” Proc. JSPE Semestrial Meet. I62, 595–596 (2013) (in Japanese).

28. D. Zhang, and L. Guan, Laser Ablation, Reference Module in Materials Science and Materials Engineering, Comprehensive Materials Processing, Vol. 4, 125-169 (2014).

29. Rashid A. Ganeev, "Laser- Surface interactions", Springer Science+Business Media Dordrecht (2014).

30. M. Sharifiana, F. Ghoveisi, and N. Firouzi Farrashbandi, "Inverse Bremsstrahlung absorption in under-dense plasma with Kappa distributed electrons", AIP Advances 7, 055107 (2017).

31. P.S. Huang and H.Y. Lai, "The effects of optical absorption coefficient on dislocation behaviors of grain boundary induced by femtosecond laser ablation", Journal of the Chinese Society of Mechanical Engineers, Vol. 31, No. 6, 477~483 (2010).

32. K. Sogiuka, M. Meunier, and A. Pique, "Laser Precision Microfabrication", Springer-Verlag Berlin Heidelberg (2010).

33. M. Koç, and T. Özel, Modern Manufacturing Processes, Wiley Online Library.

34. M. A. Green and M. J. Keevers, “Optical properties of intrinsic silicon at 300 K,” Prog. Photovolt. Res. Appl. 3, 189–192 (1995).

35. H. H. Li, “Refractive index of silicon and germanium and its wavelength and temperature derivatives,” J. Phys. Chem. Ref. Data 9, 561 (1980).

36. S. Xiao, E. L. Gurevich, and A. Ostendorf, “Incubation effect and its influence on laser patterning of ITO thin film,” Appl. Phys. A 107, 333–338 (2012).

37. F. Di Niso, C. Gaudiuso, T. Sibillano, F. P. Mezzapesa, A. Ancona, and P. M. Lugarà, "Influence of the repetition rate and pulse duration on the incubation effect in multiple-shots ultrafast laser ablation of steel," Phys. Proc. 41, 698–707 (2013).

38. J. Bonse, J. Kruger, S. Höhm, and A. Rosenfeld, "Femtosecond laser-induced periodic surface structures," J. Laser Appl. 24, 042006 (2012).

39. K. X. Pham, R. Tanabe, and Y. Ito, "Trepanning drilling of microholes on cemented tungsten carbide using femtosecond laser pulses," J. Laser Appl. 24, 032007 (2012).

40. J. Reif, F. Costache, M. Henyk, and S. V. Pandelov, "Ripples revisited: non-classical morphology at the bottom of femtosecond laser ablation craters in transparent dielectrics," Appl. Surf. Sci. 197–198, 891–895 (2002).

41. Y. Ito, Y. Morita, H. Sakashita, R. Suzuki, R. Tanabe, H. Sakurai, and K. Tada, "Determining the material structure of microcrystalline silicon from raman spectra," J. Laser Appl., 1102 (2012).

42. C. Smit, R. A. C. M. M. van Swaaij, H. Donker, A. M. H. N. Petit, W. M. M. Kessels, and M. C. M. van de Sanden, "Determining the material structure of microcrystalline silicon from Raman spectra," J. Appl. Phys. 94, 3582 (2003).

43. V. V. P. Sreenivas, M. Bülters, and R. B. Bergmann, "Microsized subsurface modification of mono-crystalline silicon via non-linear absorptions," J. Eur. Opt. Soc. 7, 12035 (2012).

44. N. M. Abdul-Ameer and M. C. Abdulrida, "Direct optical energy gap in amorphous silicon quantum dots," J. Mod. Phys. 2, 1530–1537 (2011).

45. D. Kovalev, G. Polisski, M. Ben-Chorin, J. Diener, and F. Koch, "The temperature dependence of the absorption coefficient of porous silicon," J. Appl. Phys. 80, 5978 (1996).

46. I. Miyamoto, K. Cvecek, Y. Okamoto, and M. Schmidt, "Novel fusion welding technology of glass using ultrashort pulse lasers," Phys. Proc. 5, 483–493 (2010).

47. L. Mugwagwa, D. Dimitrov, S. Matope, and I. Yadroitsev, “Influence of process parameters on residual stress related distortions in selective laser melting,” Proc. Manuf. 21, 92–99 (2018).

48. D. Grojo, A. Mouskeftaras, P. Delaporte, and S. Lei, “Limitations to laser machining of silicon using femtosecond micro-Bessel beams in the infrared,” J. Appl. Phys. 117, 153105 (2015).

49. X. Q. Liu, L. Yu, Z. C. Ma and Q. D. Chen, "Silicon Three-Dimensional Structures Fabricated by Femtosecond Laser Modification with Dry Etching", Applied Optics, Vol.56, No.8, 2157-2161 (2017).

50. S. Yadavali, D. Lee and D. Issadore, "Robust Microfabrication of Highly Parallelized Three-Dimensional Microfluidics on Silicon", Scientific Reports 9, 12213, 1-10 (2019).

51. C. M. Waits, B. Morgan, M. Kastantin, and R. Ghodssi: Microfabrication of 3D Silicon MEMS Structures Using Gray-Scale Lithography and Deep Reactive Ion Etching, Sensors and Actuators A: Physical, Vol.119, Issue 1245-253 (2005).

52. S. Lee, K. Jo, H. Keum, S. Chae, Y. Kim, J. Choi, H. H. Lee, and H. J. Kim, "Nanowall Formation by Maskless Wet-Etching on a Femtosecond Laser Irradiated Silicon Surface", Applied Surface Science, Vol. 437, 190-194 (2018).

53. S. Kiyama, S. Matsuo, S. Hashimoto, and Y. Morihira, "Examination of Etching Agent and Etching Mechanism on Femtosecond Laser Microfabrication of Channels Inside Vitreous Silica Substrates", Journal of Physical Chemistry C, Vol. 113, 11560-11566 (2009).

54. M. Pfiffer, P. Cormont, E. Fargin, B. Bousquet, M. Dussauze, S. Lambert and J. Neauport, "Effects of Deep Wet Etching in HF/HNO_3 and KOH Solutions on The Laser Damage Resistance and Surface Quality of Fused Silica Optics at 351 nm", Optics Express, Vol. 25, Issue 5, 4607-4619 (2017).

55. J. Wang, H. Niino, and A. Yabe, "Micromachining of Quartz Crystal with Excimer Lasers by Laser-Induced Backside Wet Etching", Applied Physics A, Vol. 69, No. 7, S271–S273 (1999).

56. J. Wang, H. Niino, and A. Yabe, "One-step Microfabrication of Fused Silica by Laser Ablation of An Organic Solution", Applied Physics A, Vol. 68, No. 1, 111–113 (1999).

57. X. Jia and X. Zhao, "Numerical study of material decomposition in ultrafast laser interaction with metals", Applied Surface Science, Vol. 463, 781-790 (2019).

58. Y. Shimotsuma, K. Hirao, P. G. Kazansky and J. Qiu, "Three-Dimensional Micro- and Nano-Fabrication in Transparent Materials by Femtosecond Laser", Japanese Journal of Applied Physics, Vol. 44, No. 7a, 4735-4748 (2005).

59. K. Sugioka, Y. Hanada, and K. Midorikawa, "3D Integration of Microcomponents in A Single Glass Chip by Femtosecond Laser Direct Writing for Biochemical Analysis", Applied Surface Science, Vol. 253, 6595-6598 (2007).

60. N. Liu, J. Vincent, K. Moumanis, and J. J. Dubowski: Processing of Back Surface of Si Wafers with a Pulsed Nd:YAG Laser, Journal of Laser Micro/Nanoengineering, Vol. 11, No. 2, 232-238 (2016).

61. K. P. Luong, R. Tanabe, and Y. Ito, "Machining on Rear Surface of a Silicon Substrate by An Infrared Femtosecond Laser via Non-Linear Absorption Processes", Procedia CIRP, Vol. 42, 73-76 (2016).

62. J. A. Curcio and C. C. Petty, "The Near Infrared Absorption Spectrum of Liquid Water, Journal of The Optical Society of America", Vol. 41, No. 5, 302-304 (1951).

63. T. Kobayashi, T. Wakabayashi, Y. Takushima and J. Yan, "Formation Behavior of Laser-Induced Periodic Surface Structures on Stainless Tool Steel in Various Media", Precision Engineering, Vol. 57, 244-252 (2019).

64. G. Miyagi, K. Miyazaki, K. Zhang, T. Yoshifuji and J. Fujita, "Mechanism of Femtosecond Laser Induced Periodic Nanostructure Formation on Crystalline Silicon Surface Immersed in Water", Optics Express, Vol.20, No.14, 14848-14856 (2012).